Disrupted Topological Organization of Structural Networks revealed by Probabilistic Diffusion Tractography in Tourette Syndrome Children

Wen, Hongwei; Liu, Yue; Rekik, Islem; Wang, Shengpei; Zhang, Jishui; Zhang, Yue; Peng, Yun; He, Huiguang

Published in:
Human Brain Mapping

DOI:
10.1002/hbm.23643

Publication date:
2017

Document Version
Peer reviewed version

Disrupted Topological Organization of Structural Networks revealed by Probabilistic Diffusion Tractography in Tourette Syndrome Children

Hongwei Wen[1,3a], Yue Liu[4a], Islem Rekik[5], Shengpei Wang[1,3], Jishui Zhang[6], Yue Zhang[4], Yun Peng[4*], Huiguang He[1,2,3*]

[1] Research Center for Brain-inspired Intelligence, Institute of Automation, Chinese Academy of Sciences, Beijing, China

[2] Center for Excellence in Brain Science and Intelligence Technology, Chinese Academy of Sciences, Beijing, China

[3] University of Chinese Academy of Sciences, Beijing, China

[4] Department of Radiology, Beijing Children's Hospital, Capital Medical University, Beijing, China

[5] CVIP, Computing, School of Science and Engineering, University of Dundee, Dundee, UK

[6] Department of Neurology, Beijing Children's Hospital, Capital Medical University, Beijing, China

[a] These authors contributed equally to this work

Correspondence to:

Huiguang He, Research Center for Brain-inspired Intelligence,

Institute of Automation, Chinese Academy of Sciences, Beijing, 100190, China.

E-mail: huiguang.he@ia.ac.cn

Yun Peng, Department of Radiology, Beijing Children's Hospital, Capital Medical University.

No.56 Nanlishi Road, West District, Beijing, 100045, China.

E-mail: ppengyun@yahoo.com

Running Title: Disrupted Structural Networks of TS Children

Abstract

Tourette syndrome (TS) is a childhood-onset neurobehavioral disorder. Although previous TS studies revealed structural abnormalities in distinct cortico-basal ganglia circuits, the topological alterations of the whole-brain white matter (WM) structural networks remain poorly understood. Here, we used diffusion MRI probabilistic tractography and graph theoretical analysis to investigate the topological organization of WM networks in 44 drug-naive TS children and 41 age and gender matched healthy children. The WM networks were constructed by estimating inter-regional connectivity probability and the topological properties were characterized using graph theory. We found that both TS and control groups showed an efficient small-world organization in WM networks. However, compared to controls, TS children exhibited decreased global and local efficiency, increased shortest path length and small-worldness, indicating a disrupted balance between local specialization and global integration in structural networks. Although both TS and control groups showed highly similar hub distributions, TS children exhibited significant decreased nodal efficiency, mainly distributed in the default-mode, language, visual and sensorimotor systems. Furthermore, two separate networks showing significantly decreased connectivity in TS group were identified using network based statistical (NBS) analysis, primarily composed of the parieto-occipital cortex, precuneus and paracentral lobule.. Importantly, we combined support vector machine and multiple kernel learning frameworks to fuse multiple levels of network topological features for classification of individuals, achieving high accuracy of 86.47%. Together, our study revealed the disrupted topological organization of structural networks related to pathophysiology of TS, and the discriminative topological features for classification are potential quantitative neuroimaging biomarkers for clinical TS diagnosis.

Key words: Tourette syndrome, Diffusion MRI, Probabilistic Tractography, Structural Network, Graph Theory, Topological Organization, Multiple Kernel Learning

Abbreviations: TS = Tourette syndrome, MRI = magnetic resonance imaging, DTI = diffusion tensor imaging, WM = white matter, SWM = superficial white matter, NBS = network based statistical, YGTSS = Yale Global Tic Severity Scale, SVM = support vector machine, MKL = multiple kernel learning, MK-SVM = multiple kernel support vector machine

1. Introduction

Tourette syndrome (TS) is a childhood-onset neurobehavioral disorder characterized by the presence of multiple motor and vocal tics. The typical age of onset ranges from 5 to 7 years old and the worst tic severity for most patients falls between 7 to 15 years old (Liu, et al., 2013b). Affected individuals typically have repetitive, stereotyped movements or vocalizations, such as blinking, sniffing, facial movements, or tensing of the abdominal musculature (Robertson and Kao, 2011). TS is frequently accompanied by comorbidities such as obsessive–compulsive disorder (OCD), attention-deficit–hyperactivity disorder (ADHD) and other social and behavioral disturbances (Stokes, et al., 1991).

The pathophysiological mechanism that produces tics remains elusive. However, previous neuropathological and neuroimaging studies have reported dysfunction of distinct cortico-basal ganglia circuits in relation to tic generation (Mink, 2003; Worbe, et al., 2012). Indeed, the dysfunction of cortico-basal ganglia circuits at different levels in TS patient were reveal by previous studies. Briefly, cortical structural changes were found in prefrontal, sensori-motor, anterior cingulate, parietal and temporal regions (Cherine, et al., 2010; Muller-Vahl, et al., 2009a; Peterson, et al., 2001; Sowell, et al., 2008), with altered volumes of the corpus callosum (Plessen, et al., 2004), basal ganglia (Peterson, et al., 2003) and thalamus (Miller, et al., 2010). Apart from the macroscopic volumetric changes, several studies pointed to microstructural abnormalities in white matter (WM), which extend beyond motor pathways in TS patients (Neuner, et al., 2010; Neuner, et al., 2011). Nevertheless, these studies only revealed TS related structural alterations in some individual brain regions or circuits, including importantly, a series of parallel cortico-striato-thalamo-cortical (CSTC) circuits that link specific regions of the frontal cortex to subcortical structures and provide a framework for understanding the interconnected neurobiological roots of TS (Felling and Singer, 2011). In particular, looking at the

brain as a complex network comprising highly interconnected brain regions motivates us to study TS related neurological disorders from a network perspective. The brain structural networks (Sporns, et al., 2005) could provide us with an anatomical and physiological substrate of brain functions and help us understand how the brain structures shape functional interactions (Qi, et al., 2016). Therefore, studying WM structural networks has gained a lot of popularity recently, while highlighting the urgent need to quantify WM structural networks in vivo, non-invasively, on a global scale, in order to depict the topological organization of brain structures (Parker, et al., 2014). Subsequently, this may help pin down any neurological disease-related alteration in WM structural networks.

One of the most popular noninvasive imaging techniques is diffusion MRI. This modality reveals the microstructural characteristics of white matter (WM) tracts in the brain. Specifically, diffusion tensor imaging (DTI) and diffusion MRI tractography can reliably reconstruct the major WM tracts, thereby mapping the WM integrity and structural connectivity of the human brain in vivo (Basser, et al., 1994a; Basser, et al., 1994b; Basser, et al., 2000). Many previous studies have utilized the DTI technique and diffusion measures to investigate microstructural changes in TS children (Liu, et al., 2013b; Wen, et al., 2016a). These studies have shown that structural connectivity gets disrupted in TS patients in specific WM tracts, involving the prefrontal, parietal, occipital, and subcortical WM. These findings propel the hypothesis that structural connectivity is disrupted in TS.

Although these previous studies have markedly advanced our understanding of WM alterations in TS, it remains unclear as to whether the topological organization (e.g., network global/local efficiency, small-worldness property and nodal efficiency) of WM structural networks is abnormal in TS children. With the increasing studies reconstructing human whole-brain WM networks using diffusion MRI deterministic or probabilistic tractography methods (Gong, et al., 2009a; Gong, et al., 2009b;

Iturria-Medina, et al., 2008), more interest has been shown for depicting the network-based measurements derived from brain network data. Graph theoretical analysis can provide a unique framework for the measurement of brain networks, so it has gained more popularity in the neuroimaging and brain network research fields. In particular, graph theory analysis revealed that the WM networks exhibit many crucial topological properties, such as highly connected hubs and small-worldness (Watts and Strogatz, 1998). Generally, a small-world network is defined as a network which has high clustering coefficients and short average path lengths (Telesford, et al., 2011). Small-worldness is a global network measure that quantifies the balance between integration and segregation among all the nodes in the network (Humphries and Prescott, 2006). Furthermore, the topological organization of WM networks is disrupted under pathological conditions, for example, Alzheimer's disease (Lo, et al., 2010), schizophrenia (van den Heuvel, et al., 2010; Zalesky, et al., 2010), attention-deficit hyperactivity disorder (ADHD) (Cao, et al., 2013), neuromyelitis optica (Liu, et al., 2013a) and multiple sclerosis (Shu, et al., 2011). As for TS, altered activation and functional connectivity in cortico-basal ganglia networks was found using resting state fMRI data (Werner, et al., 2011; Worbe, et al., 2012). In addition, control networks in pediatric TS show immature and anomalous patterns of functional connectivity, primarily found in the fronto-parietal network, thought to be important for online adaptive control (Church, et al., 2009). Other studies using diffusion MRI and tractography methods showed altered structural connectivity of cortico-basal ganglia networks (Cheng, et al., 2014; Worbe, et al., 2015) in adult TS patients. However, those studies only revealed functional or structural abnormalities in distinct cortico-basal ganglia circuits, and no study has previously integrated the diffusion MRI tractography method and graph theoretical analysis to examine abnormal topological organization of whole-brain structural networks in TS patients, especially in TS children.

In addition, to date, the studies on TS were mainly limited to using traditional univariate analyses (eg. t-tests) to test for group differences. The significant findings (structural or functional alterations) are only at group level which limited clinical application. Therefore, recent attention has turned toward integrating machine-learning and neuroimaging techniques to assist clinical diagnosis. Unlike group-based comparison approaches, machine-learning techniques are able to detect the fine-grained spatial discriminative patterns, which are critical for individual-based disease diagnosis (Liu, et al., 2014). Especially, many studies have applied machine learning methods to investigate brain functional or structural networks for assisting clinical disease diagnosis (Dai, et al., 2013; Dai, et al., 2012; Jie, et al., 2014; Jin, et al., 2015; Sacchet, et al., 2015), however, only a few of them (Greene, et al., 2016) are related to TS. To date, there are no reliable neuromarkers for clinical TS diagnosis, and TS is still misdiagnosed due to its complicated clinical presentation (Cavanna and Seri, 2013). Therefore, applying machine-learning algorithms to network-based features for diagnostic classification/prediction of individuals will be helpful in assisting eventual clinical diagnosis. Furthermore, the important features used to classify individuals by diagnosis also hold promise for further refinement of the classification methods to ultimately predict prognosis and treatment responses (Greene, et al., 2016).

In the present study, we used diffusion MRI probabilistic tractography and graph theory to investigate the topological organization of whole-brain structural networks in drug-naive TS and healthy children, and their relation to clinical features. In our study, we used drug-naive subjects to exclude the effects of stimulants, as previous studies have suggested that stimulants can significantly influence the structure and function of central nervous system in TS (Golden, 1977). In this paper, we aimed to investigate whether TS children would show abnormal global and regional topological properties, disrupted nodal efficiency, altered structural connectivity between nodal regions in the whole-brain WM networks and

whether these topological changes would significantly correlate with the clinical characteristics of TS children. We assumed that the brain structural network in both TS and healthy children could follow a small-world organization, which was investigated using graph theoretical analysis to identify the differences in global and regional topological properties of brain structural networks between TS and healthy children. We hypothesized that TS children may have a disrupted topological organization of WM structural networks, involving importantly, the basal ganglia and cortical frontal areas, as previous studies revealed that microstructural dysfunction measured by DTI in component regions of the fronto-striato-thalamic (FST) circuit contributes to the pathophysiology in TS (Müller-Vahl, et al., 2014; Makki, et al., 2008). Moreover, to enhance our contributions to assisting the clinical TS diagnosis, we investigated using the complementary topological properties (global, nodal, edge) of WM structural networks as features to accurately discriminate TS children from controls. We employed the multiple kernel learning (MKL) frameworks in our previous study (Wen, et al., 2017a) to fuse these complementary network-based features, and the most discriminative features for classification, which are highly related to pathophysiology of TS, will be potential important neuroimaging biomarkers for assisting the clinical TS diagnosis.

2. Materials and Methods

2.1 Subjects

44 TS patients were recruited from outpatient clinics in Beijing Children's Hospital from July 2012 to May 2015 (age: 8.98±3.114 years, range: 3–16 years; 11 female). All the patients met DSM-IV-TR (Diagnostic and Statistical Manual of Mental Disorders, 4th Edition, text revision) criteria for TS. We also included 41 age and gender matched health controls in our study (age: 10.27±3.18 years; range: 3–

15 years; 15 female). The child psychiatrist (chief physician) in our hospital did outpatient interview to make differential diagnosis of psychiatric comorbidities for child subjects, based on the exclusion criteria of psychiatric disorders. The exclusion criteria of psychiatric disorders were established according to the Chinese Classification of Mental Disorders (currently on a third version, the CCMD-3), published by the Chinese Society of Psychiatry (CSP), and used as a clinical guide in China for the diagnosis of mental disorders. The diagnostic criteria of CCMD-3 also refer to the research criteria of DSM-IV (Chen, 2002). Then the professional neurologists made differential diagnosis of OCD and ADHD using scales. Briefly, we used a clinical interview and the Children's Yale-Brown Obsessive Compulsive Scale (CY-BOCS) (Scahill, et al., 1997) to diagnose OCD and used the German short version of Wender Utah rating scale (WURS-k, translated to Chinese) (Retz-Junginger, et al., 2003) to diagnose ADHD. Patients fulfilling OCD criteria or other co-morbidities were excluded from the study. Tic severity for all patients was rated using the Yale Global Tic Severity Scale (YGTSS) (Leckman, et al., 1989) and ranged from 10 to 79 ([mean±SD]: 51.20±19.38). The duration of TS ranged from 3 months to 5 years ([mean±SD]: 1.73±1.44 years). For subjects who had course less than 1 year, their diagnosis was made by follow-up call and they were all finally diagnosed exactly as TS by our professional neurologists and psychiatrists. Following the study approval by Beijing Children's Hospital review board, written informed consent was obtained from all the parents/guardians according to the Declaration of Helsinki. Details of the patients are shown Table 1.

[Insert Table 1 about here]

2.2 Data acquisition

Magnetic resonance imaging was acquired using a 3T MR scanner (Gyroscan Interna Nova, Philips,

Netherland). Head positioning was standardized using canthomeatal landmarks. The head was stabilized with foam pads to minimize head movements. Patients were instructed to suppress tics and minimize head movements during scanning as much as possible. All children under seven years old were kept asleep during the MR scan. Axial three-dimensional diffusion tensor imaging (DTI) was acquired from all the subjects. DTI was performed using the following protocol: spin-echo diffusion-weighted echo-planar imaging sequence, 2mm slice thickness, no inter-slice gap, repetition time = 4300ms, echo time = 95ms, field of view (FOV) =255×255mm, reconstructed image matrix = 336×336. Diffusion MRI images were obtained from 30 non-collinear directions with a b value of 1000 s/mm^2. 3D T1-weighted imaging were performed with axial three-dimensional-Fast Field Echo (3D FFE) sequence with the following parameters: repetition time (TR) = 25ms, echo time (TE) = 4.6ms, flip angle = 30°, reconstructed image matrix = 256×256, field of view (FOV) = 200×200mm, slice thickness = 1mm.

2.3 Preprocessing

Following DTI acquisition, we used the FMRIB's Diffusion Toolbox (FDT2.0) within FSL v4.1 (http://www.fmrib.ox.ac.uk/fsl) for DTI processing. As Differences in head motion between groups can induce spurious group differences (Yendiki, et al., 2014), prior to the estimation of diffusion, we used the same preprocessing pipeline as in the previous TS study (Wen, et al., 2016a) to perform corrections for distortions due to eddy currents and head motion. In detail, we used the ***eddy*** tool in FDT, which is a tool to correct for eddy current-induced distortions and subject movements in diffusion data. It simultaneously models the effects of diffusion eddy currents and movements on the image. It also performs outlier detection to identify slices where signal has been lost as a consequence of subject

movement during the diffusion encoding, and permits replacement of the outliers with distortion-free data. For each participant, 30 DTI volumes with 1000s/mm^2 b-value were first affinely registered to the b_0 volume. After running motion and eddy correction, we extracted the head motion parameters with the displacement, rotation and translation information for each subject. We found no significant between-group differences for any head motion parameter using the two-sample t test (Table 1). Non-brain voxels were removed using Brain Extraction Tool (BET) of FSL; a fractional intensity threshold of 0.25 was selected, resulting in a brain-extracted 4D image and a binary brain mask for each subject. We then used the eddy-corrected 4D data and corresponding brain mask to fit the diffusion tensor model at each voxel using the FDT. Eigenvalues of diffusion tensor matrix (λ_1, λ_2, λ_3) were obtained and maps of fractional anisotropy (FA) were generated.

2.4 Network construction

Nodes and edges constitute the two basic elements of a network. In the present study, we defined all of the network nodes and edges using the following steps.

2.4.1 Network node definition.

We defined the network nodes strictly in accordance with the procedure described previously (Gong, et al., 2009a; Gong, et al., 2009b) and was performed here using SPM8 (http://www.fil.ion.ucl.ac.uk/spm). Briefly, individual T1-weighted images were coregistered to the b_0 images in the DTI space. Then, the transformed T1 images were then nonlinearly transformed to the ICBM152 T1 template in the MNI space. The inverse transformations were used to warp the automated anatomical labeling (AAL) atlas (Tzourio-Mazoyer, et al., 2002) from the MNI space to the DTI native space. Of note, the

nearest-neighbor interpolation method was used to preserve discrete labeling values. Using this procedure, we obtained 90 cortical and subcortical regions (45 for each hemisphere; Table 2), each representing a node in the network (Fig. 1).

[Insert Table 2 about here]

2.4.2 Network edge definition.

To define the connections (edges) between brain regions, we performed probabilistic tractography using the FMRIB Diffusion Toolbox (FSL, version 4.1; http://www.fmrib.ox.ac.uk/fsl). Firstly, we used the bedpostx tool in FSL to run Markov Chain Monte Carlo sampling, in order to estimate distributions on diffusion parameters at each voxel, which allows to model crossing fibers within each voxel of the brain. Secondly, we used the probtrackx tool in FSL to perform probabilistic tracking. Briefly, we repetitively performed 5000 sampling from the distributions of voxel-wise principal diffusion directions, each time computing a streamline through these local samples to generate a probabilistic streamline fiber. For a seed region, 5000 × n streamline fibers were sampled; n is the number of voxels in the seed region. The number of streamline fibers passing through a given region divided by 5000 × n is calculated as the connectivity probability from the seed region to the given region. In our study, each brain region in AAL template was selected as the seed region, and its connectivity probability to each of the other 89 regions was calculated. Notably, the probability from i to j is not necessarily equivalent to the probability from j to i because the tractography is dependent on the seeding location. However, these two probabilities are highly correlated across the brain regions for all subjects in our study (all Pearson $r > 0.76$, $p < 0.05$). Thus, we defined the unidirectional connectivity probability P_{ij} between region i and region j by averaging these two probabilities as in (Cao, et al., 2013).

Finally, to define the network edges, we computed $w_{ij} = P_{ij}$ as the weight between brain regions i and j. For each subject, a 90 × 90 symmetric weighted network was constructed. To remove spurious connections, we applied a set of thresholds ranging between 0.01 and 0.1 at equal intervals of 0.0025 empirically based on a previous structural network study (Cao, et al., 2013). Specifically, two brain regions were considered disconnected if the connection weight w_{ij} was below a given threshold. The flowchart for structural network construction was shown in Fig. 1.

[Insert Figure 1 about here]

2.5 Network topological attributes analysis

For the weighted WM networks (G) at each threshold, we calculate two sets of network topological attributes, including both global and local network properties. The general descriptions of these network properties are given below.

Global network properties

S_p: network strength (mean degree). S_p is the strength of the network, which is defined as the mean degree of all the regions in the brain network.

E_{glob}: network global efficiency. E_{glob} is defined as the inverse of average shortest path length. It reflects the network efficiency in transferring information, which can be computed as follows:

$$E_{\text{glob}}(G) = \frac{1}{N(N-1)} \sum_{i \neq j \in G} \frac{1}{L_{ij}} \tag{1}$$

E_{loc}: network local efficiency. E_{loc} is defined as the average value of all regions' local efficiency. It reflects system redundancy and tolerance to attack, which can be computed as follows:

$$E_{\text{loc}}(G) = \frac{1}{N}\sum_{i \in G} E_{\text{glob}}(G_i) \tag{2}$$

L_p: the shortest path length. L_{ij} is defined as the length of the path for node i and node j with the shortest length. L_p is the shortest path length of network G, which can be computed as follows:

$$L_p(G) = \frac{1}{N(N-1)}\sum_{i \neq j \in G} L_{ij} \tag{3}$$

C_p: the clustering coefficient. C(i) is defined as the clustering coefficient of a node i, equal to the ratio between the existing number of edges among the neighbors of the node i and the maximum possible number of connections among these neighbors, which can be computed as follows:

$$C(i) = \frac{2}{k_i(k_i-1)}\sum_{j,k} (\overline{w}_{ij}\,\overline{w}_{jk}\,\overline{w}_{ki})^{\frac{1}{3}} \tag{4}$$

where k_i is the degree of node i, and $\overline{w}_{ij}$ is the edge weight, which is scaled by the mean of all edge weights to control each participant's cost at the same level. C_p is defined as the average clustering coefficient over all nodes, It quantifies the cliquishness and reflects the extent of local interconnectivity.

To examine the small-world properties, the C_p and L_p of the brain networks were compared with those of random networks. In this study, we generated 100 matched random networks, which had the same number of nodes, edges, and degree distribution as the real networks (Maslov and Sneppen, 2002). To preserve the weight distribution of the network, we retained the weight of each edge during the randomization procedure.

λ: the normalized shortest path length. $\lambda = L_p^{real}/L_p^{rand}$, L_p^{rand} is the mean shortest path length of 100 matched random networks.

γ: the normalized clustering coefficient. $\gamma = C_p^{real}/C_p^{rand}$, C_p^{rand} is the mean clustering coefficient of 100 matched random networks.

σ: the small-worldness. σ=γ/λ, which reflects the balance between integration and segregation among all the nodes in the network. The network with small-worldness is a kind of network with both high clustering coefficient and low shortest path length.

Regional nodal characteristics

E_{nodal}(i): nodal efficiency. E_{nodal}(i) is the regional efficiency of node i and indicates the nodal (regional) characteristics of the WM networks, which can be computed as follows:

$$E_{\text{nodal}}(i) = \frac{1}{N-1} \sum_{i \neq j \in G} \frac{1}{L_{ij}} \tag{5}$$

where L_{ij} is the shortest path length between node i and node j in the network G, and E_{nodal}(i) measures the average shortest path length between a given node i and all of the other nodes in the network.

Similar to previous studies (Zhang, et al., 2015; Zhang, et al., 2011), we also calculated the area under the curve (AUC) for each network metric (global and local topological properties) to provide a summarized scalar independent of single threshold selection. Of note, we used the AUC value of the nodal efficiency across thresholds for the analysis of regional properties, defining brain hubs and significant altered nodes.

2.6 Network based statistical analysis

To localize specific pairs of brain regions in which structural connectivity was altered in TS children, we used a method called network based statistical (NBS) analysis (Zalesky, et al., 2010) (http://www.nitrc.org/projects/nbs/), which identifies the between-group differences in pair-wise edge (or connection) weight under a series of probability thresholds (0.01–0.1, interval = 0.0025). The basic idea of the network-based statistics is to correct for multiple comparisons by testing for evidence

against the null distribution at the level of graph components, rather than at the level of individual connections (Hong, et al., 2014). Briefly, the two-sample t-tests were firstly performed to test for between-group differences in the connections of the 90*(90-1)/2=4005 unique regional pairings. Then, a most liberal primary threshold (p=0.01) (Marques, et al., 2015; Zhu, et al., 2016) in NBS analysis was applied to the t statistic computed for each link to define a set of suprathreshold links, among which any connected components and their size (number of links) were then determined. The t value was uniquely determined, when the degrees of freedom (N1 - 1 + N2 - 1 for independent samples, in our study, 41-1+44-1=83), and significance level (p value = 0.01 in our study) were determined. The t=2.372 in our study can be calculated based on the table for T distributions which is provided in the supplementary material. Secondly, the null distribution of connected component size was derived using a nonparametric permutation approach (10,000 permutations) in order to estimate the significance for each component, then the threshold (p=0.05) was used to generate suprathreshold links (Cao, et al., 2013). Finally, the corrected p value was estimated for each component as the proportion of permutations that yielded a larger component or one of equal size. This NBS method has recently been used to identify abnormal brain connectivity circuitry in other diseases such as ADHD (Cao, et al., 2013; Hong, et al., 2014) and depression (Zhang, et al., 2011). The NBS method aims to identify the connected sub-networks in the connectivity matrix that significantly differ between groups which would offer greater statistical power (Verstraete, et al., 2011) and reveal more differences that probably have been overlooked with the false discovery rate (FDR) correction (Li, et al., 2013).

2.7 Linking changes to clinical variables

For all significantly altered nodal efficiencies in regional topological analysis, and significantly altered

structural connections (SC) in NBS analysis, we examined the correlations between these significantly altered network metrics and the clinical variables in the TS group. To lessen the concern that the between-group differences of age, gender and head motion parameters (though all the metrics were not significantly different between groups) might significantly affect the analysis results, we performed partial correlation analyses (dependent variables: network metrics; independent variables: tic severity score/YGTSS or tics duration) using SPSS 19.0. Age, gender and six head motion parameters (x, y, z rotation and x, y, z translation) were calculated as covariates.

2.8 Combining complementary network-based features for individual classification using multiple kernel learning

Apart from revealing disrupted topological properties of WM structural networks in TS using univariate approach, we also investigate using multiple levels of network topological properties as features to accurately discriminate TS children from controls. We used the original network characteristics including 8*37 global properties (across all 37 thresholds), 90 nodal properties (AUC value), 4005 (90*89/2) edge weights,, respectively, as features for subsequent classification. As in our previous study (Wen, et al., 2017a), the SVM-RFE (Guyon, et al., 2002) algorithm was used for feature selection. Then, classification was performed using the support vector machine (SVM) algorithm (Cortes and Vapnik, 1995) with a radial basis function (RBF) kernel. To estimate optimal values for the two SVM parameters, the complexity or cost constant ($c>0$) and kernel width ($\gamma>0$), we used a grid search in the range of $c=2^{-4}, 2^{-1}, ..., 2^{4}$ and $\gamma=2^{-8}, 2^{-9}, ...,2^{2}$, with 10-fold CV to evaluate the goodness of SVM parameters.

To further integrate the complementary information of these three kinds of network metrics (global, nodal, edge), we employ the same multiple kernel learning (MKL) frameworks (Wen, et al., 2017a) to fuse these features. The MKL algorithm can automatically search the optimal combination of the kernel matrix of these features to form an integrated kernel matrix (assigning weight to each kernel matrix), which outperforms the use of single kernels. The output of MKL is defined as:

$$y_i = \sum_k \beta_k \left(\sum_j \lambda_j^k y_j K_k \left(x_j^k, x_i^k \right) \right) + b \tag{6}$$

where k denotes the k-th kind of feature; y_i denotes the corresponding class label of i-th subject; K_k is the kernel matrix; β_k is the sub-kernel weight; λ_j^k is the Lagrange parameters; x_j^k is the support vector of training set; and x_i^k is the feature vector of the i-th test sample.

We used the same optimal feature subset and SVM parameters determined earlier for each single type of features (global, nodal, edge). Our classification framework and validation experiments were implemented in Matlab using LIBSVM (v3.1.2, www.csie.ntu.edu.tw/~cjlin/libsvm/) for the SVM classifier and Shogun (v3.2.0, www.shogun-toolbox.org/) for the MKL framework.

In our study, the same nested cross-validation strategy (Wen, et al., 2017a) (Fig. 2 shows the detailed flow chart) was used to evaluate the classification performance, which was considered as the excellent estimation of generalization (Wilson, et al., 2009). The statistics we used to evaluate our classification algorithm performance are accuracy, sensitivity, specificity and the area under the curve for the receiver operated characteristic curve (AUC ROC). Accuracy is defined as (TP+TN)/(TP+TN+FN+FP) where TP = True Positive, TN =True Negative, FP = False Positive and FN = False Negative. Sensitivity is defined as TP/(TP+FN) and Specificity is defined as TN/(FP+TN).

[Insert Figure 2 about here]

3. Results

3.1 Alterations in the global properties of WM networks in TS

Both TS patients and controls showed a small-world organization of WM networks characterized by $\gamma>1$ and $\lambda\approx1$ (Fig. 3). However, compared with controls, TS children had significantly decreased C_p, λ, global and local efficiency, increased L_p, γ and σ in the WM networks for different thresholds. All the significant p value (<0.05) were derived after FDR correction (Benjamini and Hochberg, 2015). Moreover, the AUC value of the shortest path length L_p significantly increased in TS group compared to control group. There were no significant differences between groups in other network metrics (Fig. 3; Table 3).

[Insert Figure 3 about here]

[Insert Table 3 about here]

3.2 Alterations in the regional properties of WM networks in TS

We identified the hub regions of the WM networks for each group. The nodes were considered brain hubs if their nodal efficiencies (AUC value) were at least 1 standard deviation (SD) greater than the average nodal efficiency of the network.

We found that the TS and control groups showed highly similar hub distributions, with core regions mainly in the cingulate gyri (both anterior, middle and posterior part), occipital (bilateral cuneus, superior occipital gyrus, left middle occipital gyrus) and parietal cortices (bilateral precuneus) (Fig. 4; Table 4).

[Insert Table 4 about here]

Further statistical analysis revealed that TS group had significant reduced nodal efficiency mainly in the bilateral inferior occipital gyrus and superior parietal gyrus, left lingual gyrus, left inferior frontal gyrus (opercular, triangular part), left parietal cortices (supramarginal gyrus and inferior parietal gyrus) and left temporal cortices (fusiform gyrus and hippocampus)(Table 5). No node region showed significant increased nodal efficiency. Of note, the regions that showed significant reduced nodal efficiency in TS group were not the hubs regions (Fig. 4). In addition, for TS group, we found no significant correlations between nodal efficiency and clinical variables in any disrupted region.

[Insert Table 5 about here]

[Insert Figure 4 about here]

3.3 Decreased regional connectivity in TS revealed by NBS analysis

Using the NBS analysis, two separate networks showing significantly decreased connection strengths in TS children compared with healthy children were identified (p values < 0.05, NBS corrected). The first network (network 1 in Table 6) comprised 6 links, involving 7 different brain regions, which locate in the right occipital gyrus, superior parietal gyrus, cuneus, precuneus, lingual gyrus (p values < 0.05, NBS corrected; Fig. 5). The second network (network 2 in Table 6) was composed of 4 links, involving 5 different brain regions, which locate in the left middle occipital gyrus, superior parietal gyrus, precuneus, bilateral paracentral lobule (p values < 0.05, NBS corrected; Fig. 5). The strengths, percentages, and frequencies of these decreased WM connections across thresholds are shown in Table 6. We did not identify any network with significantly increased connectivity in the TS group. In addition, for TS group, we found no significant correlations between connection strength and clinical

variables in any disrupted links.

[Insert Table 6 about here]

[Insert Figure 5 about here]

3.4 Classification results using multiple kernel learning

We used SVM classifier, which classifies subjects into TS group and healthy control groups. The classification accuracies of using a single type of features (global, nodal, edge) and combining features (using MKL) are showed in Table 7. To avoid potential lack of robustness and stability of classification based on one-time random partitioning in CV, we repeated the nested CV procedure for twenty times. The highest classification performance with mean (±SD) accuracy (86.47±3.71%), sensitivity (85.57±4.38%), specificity (87.44±4.13%), and ROC AUC (92.62±3.35%) were achieved on the combined features using MKL, which was demonstrated to perform better than a single type of features. Fig. 6A shows the receiver operating characteristic (ROC) curves of all the methods.

As the highest accuracy was achieved when combining features, the current work also identified the most discriminative network features for TS classification. Since the feature selection in each fold is performed based only on the training set, the selected features could differ slightly across different cross-validation folds. Therefore, we summed the counts of each feature selected by our proposed method over the 20 rounds nested 10-fold CV. The frequencies of the top ten features for each type of network properties were provided in Table 8.

For the purpose of visualization, we display the brain regions with nodal efficiencies identified as discriminative features (with frequency >0.2) for TS classification using MKL in Fig. 6B.

[Insert Table 7 about here]

[Insert Table 8 about here]

[Insert Figure 6 about here]

4. Discussion

In the present study, we used probabilistic diffusion tractography and graph theory to investigate the topological organization of the WM structural networks in drug-naive TS children compared with healthy children. Both TS and healthy children showed small-world properties of the WM networks, characterized by high local clustering and short path length, which are in accordance with previous WM network studies in healthy children (Cao, et al., 2013). Despite the common small-world topology, TS children showed decreased global and local efficiency and increased shortest path length. Although both TS and control groups showed highly similar hub distributions, TS children exhibited significant decreased nodal efficiency, primarily in the inferior frontal gyrus, inferior parietal gyrus (Wittfoth, et al., 2012) and hippocampus (Peterson, et al., 2007), and previous studies also revealed structural alterations of these regions in TS. Furthermore, TS children exhibited decreased network connectivity, primarily in the occipital gyrus, superior parietal gyrus, cuneus, precuneus, and lingual gyrus. Finally, no significant correlation between network metrics and clinical variables was found, using age, gender and head motion parameters as covariates. Of note, though age is not significantly different between groups, there may still be a between-group difference ($p=0.062$) in age. Therefore, age was calculated as a covariate to eliminate its potential impact on the correlation analysis results. Together, our study showed the disruption of topological organization in WM networks in TS children.

4.1 Altered global properties in the WM networks in TS

In the present study, we characterized the small-world topology of the WM networks in both TS and healthy children, using the probabilistic tractography method to map whole-brain WM connectivity, which has advantages in tracking crossing and splitting fiber bundles compared with deterministic tractography methods (Behrens, et al., 2007). Both TS and healthy children had brain networks with small-worldness property. Small-worldness property means that the network has high efficiency in information processing and transfer (Sporns and Honey, 2006). Previous studies have proven the small-worldness property of the brain structural network via diffusion MRI (Gong, et al., 2009a; Hagmann, et al., 2007; Iturria-Medina, et al., 2008).

Although the structural networks in TS children showed prominent small-world topology, the global and local efficiencies were significantly decreased, while short path length and small-worldness were significantly increased at a series of threshold compared with controls. The global efficiency reflects the information transfer between remote cortical regions, and it is mainly associated with long-range connections. The local efficiency is predominantly related to the short-range connections between neighboring regions. Decreases in both global and local efficiencies reflect disrupted topological organizations of the WM networks in TS patients, which could be due to impaired structural connections. Many DTI studies provided direct evidence for disrupted structural integrity in various WM tracts in TS children, such as the corticospinal tract, the superior/inferior longitudinal fasciculus, the superior/inferior fronto-occipital fasciculus, the anterior thalamic radiation and the corpus callosum (Wen, et al., 2016a). Evidence from a magnetization transfer ratio (MTR) study also showed WM reductions in the inferior frontal gyrus and cingulate gyrus in TS patients (Muller-Vahl, et al., 2009b), and previous post-mortem study (Thomas, et al., 2004) proved MTR reductions correlate with myelin

and axonal loss in the WM. So, our results showed that reduced white matter integrity is associated with TS children (Plessen, et al., 2006; Wen, et al., 2016a) from a network perspective, and the reduced global and local efficiencies in TS group may indicate a disturbance of the normal balance in their structural brain network, which tends to have a more randomized configuration (Peng, et al., 2014).

Moreover, significantly increased short path length and small-worldness were also found for different thresholds, especially the AUC value of shortest path length was significantly increased in TS group compared to control group. Increased short path length suggests reduced efficiency of parallel information transfer in the WM networks in TS children. Since the small-world connectivity model reflects an optimal balance between local specialization and global integration, the significant increased short path length and small-worldness in the structural networks of TS children could indicate less optimal organization of the brain networks, possibly as a consequence of reorganization secondary to cortical injury (Liu, et al., 2012).

4.2 Highly similar hub distributions between TS and controls

In addition to noting prominent small-world topology in both TS and healthy children, we also found that the TS and control children have highly similar hub distributions, with core regions mainly in the cingulate gyri (both anterior, middle and posterior part), occipital (bilateral cuneus, superior occipital gyrus, left middle occipital gyrus) and parietal cortices (bilateral precuneus). Our results suggest that the key regions of structural network are conserved throughout the development process and the small-world networks can tolerate developmental alterations or disease (He, et al., 2009; Supekar, et al., 2009).

Of note, our results showed that the bilateral anterior, posterior cingulate gyrus and precuneus were hub

regions in both groups. These regions were in the default-mode network (DMN), one of the most described resting-state networks (RSNs). DMN activates when an individual is awake and alert, but is not actively involved in an attention demanding or goal-directed task. Although the DMN concept is derived from resting-state functional MRI, some recent studies have combined fMRI and DTI in healthy participants (Greicius, et al., 2009; Horn, et al., 2014; Oort, et al., 2013; Supekar, et al., 2010), reporting significant correlations between the DMN structural and functional connections. A previous WM network study also showed similar hubs regions within DMN in healthy children (Cao, et al., 2013) as ours. In particular, bilateral precuneus with DMN were found to be consistent rich-club hub regions in both TS and healthy children (Wen, et al., 2017c). Our finding of highly similar hub distributions between groups is also largely consistent with this study.

4.3 Distributed regions with altered efficiency in TS

In the present study, we observed several brain regions with reduced efficiency in TS children, primarily in the occipital gyrus (bilateral inferior occipital gyrus, left ingual gyrus), left inferior frontal gyrus (opercular, triangular part), left parietal (supramarginal gyrus, superior and inferior parietal gyrus) and left temporal cortices (fusiform gyrus and hippocampus). These regions are key nodes in the brain networks and exhibit structural and functional abnormalities in TS (Bush et al., 2005; Seidman et al., 2005), which were involved in visual, default-mode, language and sensorimotor related areas.

Firstly, reduced nodal efficiencies were also found in several occipital regions (inferior occipital gyrus and lingual gyrus) that are important for visual processing. Few studies have identified structural abnormalities in the TS patients in the visual regions. Smaller inferior occipital volumes were found in TS subjects (Peterson, et al., 2001) and WM volumes decreased in left lingual gyrus (Liu, et al., 2013b).

Of note, the nodal efficiency of right inferior occipital gyrus was also reported to be one of the discriminative structural network features for differentiating early TS children form healthy children (Wen, et al., 2016b). Despite these advances, very little is known about the alterations in the topological organization of network in visual regions. Thus, our results provide further evidence for the structural disruption of the visual system in TS patients.

Secondly, we observed a decreased nodal efficiency in the structural networks of TS children in several default-mode regions (hippocampus and inferior parietal lobules). These regions represent core components of the DMN, which has been reported to be highly related to tic generation in adult TS patients (Neuner, et al., 2014). Cui et al. (Cui, et al., 2014) found that TS children showed significantly decreased ALFF in the inferior parietal lobules (IPL). Furthermore, functional abnormalities in the IPL have been described before (Swick, et al., 2011). Hippocampal volume alterations were also been found in TS boys and structural changes in hippocampus might indicate an involvement of temporolimbic pathways of the CSTC in the syndrome (Ludolph, et al., 2006). Previous studies combined DTI tractography with resting-state functional connectivity MRI to demonstrate that resting-state functional connectivity could reflect structural connectivity in the DMN (Greicius, et al., 2009). Thus, our results are in agreement with these previous findings.

Thirdly, reduced nodal efficiencies were observed in several frontal regions (IFGoperc, IFGtriang) that are key components for language processing. The IFGoperc and IFGtriang, comprising Broca's area, especially in the left hemisphere, are known to be important for language synthesis. Structural and functional changes in the inferior frontal gyrus (IFG) regions in TS patients have been reported in previous neuroimaging studies (Ganos, et al., 2014; Wittfoth, et al., 2012). Apart from playing a key role in tic inhibition (Ganos, et al., 2014), the left IFG has also been associated with aspects of

language processing (Liakakis, et al., 2011). Particularly, several previous studies have indicated that the left IFG (eg. IFGoperc.L and IFGtriang.L) are important for elaborated semantic inhibition (Zhu, et al., 2013; Zhu, et al., 2009). In this study, 28 of 44 TS patients exhibited vocal tic (including humming, grunting, or saying actual words, usually in an explosive fashion and the words may involve curses), which supports for our findings of the abnormalities in the language areas.

Finally, we observed reduced nodal efficiencies in the bilateral superior parietal lobe, which is related to sensorimotor association functions. A previous study (Wolpert, et al., 1998) suggests that the superior parietal lobe is critical for sensorimotor integration, by maintaining an internal representation of the body's state. Buse et al. (Buse, et al., 2015) found decreased prepulse inhibition related BOLD activity in TS boys in the superior parietal cortex. Bohlhalter et al. (Bohlhalter, et al., 2006) showed that at the beginning of tic action, significant fMRI activities were found in sensorimotor areas including the superior parietal lobule bilaterally and cerebellum. Morphological studies also reported increases in GM volumes in left superior parietal lobule (Liu, et al., 2011) or cortical GM volumes in superior parietal lobule showing significant correlations with clinical scores (Wittfoth, et al., 2012). These findings suggest that structural and functional changes exist in the sensorimotor related areas in patients with TS, which provides support for our findings.

Of note, many TS children were reported to also have fine motor control and visual-motor integration impairment. A neuropsychological model of visual-motor integration skill was proposed and tested in 50 TS children and 23 unaffected age-matched control children (Schultz, et al., 1998), which suggests that the integration of visual inputs and organized motor output is a specific area of neuropsychological weakness among TS children. Our studies revealed regional efficiencies decreased in visual and motor related areas in TS children. This finding reflects a less optimal balance between local specialization

and global visual-motor integration in structural networks, which may weaken visual-motor integration functioning in TS children.

4.4 Decreased connectivity of parieto-occipital association areas in TS

We observed aberrant structural connectivity in two networks in TS patients. One network with decreased connection strengths was primarily composed of the bilateral occipital gyrus, superior parietal gyrus and right cuneus. Decreased structural connectivity means biologically the decreased WM connection probabilistic between regions, and decreased WM connection probability or fractional anisotropy (FA) values are usually associated with disease pathology (Cao, et al., 2013). Superior occipital gyrus follows the superior edge of the lobe and merges with cuneus on the medial surface of the occipital lobe, and this link connecting the superior occipital gyrus to the cuneus showed the significantly decreased structural connection strength in NBS analysis. At the level of the parieto-occipital fissure, the superior parietal gyrus is linked to the superior occipital gyrus by a transitional area called arcus parieto-occipitalis, and this link also showed significantly decreased structural connection strength.

Previous studies using structural MRI in TS provided some evidence for parieto-occipital anatomical abnormalities. TS children (5–18 years) were found to have larger cortical volumes in parieto-occipital regions (Peterson, et al., 2001) compared to unaffected children, which also suggest a possible connection that increased volumes of parieto-occipital cortex are significantly correlated with tic severity. However, at present, it is unclear whether, or how, larger parieto-occipital volumes in TS children affect the abnormal structural connectivity in those regions. In addition to volumetric approaches, DTI has also been used to investigate, indirectly, the microstructural properties of the

regions in TS. The previous diffusion MRI studies found decreased FA and increased MD in superficial WM regions of parieto-occipital cortex in TS children (Wen, et al., 2016a) and suggested that a disrupted myelination mechanism underlie the abnormalities. Increased MD value or decreased FA values could reflect reduced myelination, fewer axons, or atypical organization of axons within the WM tract. Considering the somewhat consistent finding of increased cortical volumes, increased MD value or decreased FA value in TS children, those microstructural differences would likely coincide with altered cortical volumes. Our study made a meaningful exploration of this issue, providing interesting and potentially valuable information about the regional morphology, WM properties and whole-brain structural networks in TS children.

4.5 Decreased connectivity of precuneus, paracentral lobule in TS

The second network component with decreased WM connections in TS primarily involved the precuneus and paracentral lobule. As the precuneus is a part of the superior parietal lobule forward of the occipital lobe (cuneus), the precuneus linking the superior parietal gyrus and paracentral lobule were two important connections with significantly decreased connectivity in our study. The precuneus has been suggested to be the hub of the DMN that is activated during "resting consciousness" in which people do not engage intentionally in sensory or motor activity (Cavanna, 2007). Bullmore et al. also proposed that its functions link to its role as a central and well connected "small-world network" hub between parietal and prefrontal regions (Bullmore and Sporns, 2009). Furthermore, our result showed that the precuneus is also a structural hub and its structural connection with parietal regions is significantly disrupted in TS children. The previous study (Wen, et al., 2016a) also reported significantly reduced FA value or increased RD value in precuneus WM, which reveals microstructural

abnormalities in this region and is in line with our finding.

Of note, the precuneus, inferior parietal gyrus (IPL), median cingulate (DCG) and frontal cortex are key components in the 'fronto-parietal' network. A previous study (Church, et al., 2009) revealed that pediatric TS patients showed immature and anomalous patterns of functional connectivity, primarily in the fronto-parietal network, which is important for online adaptive control. Our results also revealed regional efficiencies decrease in the IPL and frontal cortex. The disrupted structural connectivity in fronto-parietal network may lead the functional underconnectivity (Church, et al., 2009), which could affect the communication and coordination of activity between the cerebellum, frontal cortex and parietal cortex, related to distinctive symptoms in different developmental disorders. Furthermore, a previous WM structural networks study (Wen, et al., 2017b) also found that the nodal topological properties of precuneus and paracentral lobule were discriminative features for TS classification, which could be used as biomarkers for TS pathology .

4.6 The MKL framework combining complementary network-based features has stronger classifying ability

Identification of objective neuroimaging biomarkers is of great interest as it could, ultimately, assist clinical decisions for individual patients. To date, TS diagnosis mainly depends on the qualitative description of symptoms as there is no hallmark imaging abnormality in routine examination or other reliable diagnostic biomarkers (Felling and Singer, 2011). Specially, network-based biomarkers can capture the role of brain network structure in a phenotype and study the role of known subsystems for a given disorder, thereby defining new potential beneficial neuroimaging biomarkers. With this consideration, a previous study (Greene, et al., 2016) used resting state functional connectivity (RSFC)

MRI to construct the RSFC networks by calculating the correlation (r value) of each ROI's time-course with every other ROI's time-course. The functional connections (r value) were directly regarded as features and fed into SVM for distinguishing TS children from healthy children. The peak accuracy reached 74% with sensitivity of 76% and specificity of 71%. Nevertheless, since the human brain is a very complex and rich network, solely relying on low-level original connectivity values as features cannot capture high-level topological properties of this network. In addition, the conventional single-kernel SVM used for classification cannot optimize kernel weights of different types of features, therefore, cannot reflect the different discriminative ability of features for classification.

In this study, we combined multiple levels of original topological properties of WM structural networks, and then used the MKL framework to fuse the complementary network-based features. We implemented feature selection algorithm on the original features without between-group statistical comparison to select significantly altered features firstly, which can ensure SVM results have good generalization ability as in our previous study (Wen, et al., 2017a). The classification performances with higher accuracy, sensitivity and specificity in our study than the previous study (Greene, et al., 2016) have shown that the integration of multiple kernels not only increases the classification accuracy but also enhances the interpretability of the results. For each feature, we also counted its selection frequency by SVM-RFE method in nested CV procedure, to reveal the discriminative features for classification. Our results showed that the features with significant between-group difference might differ from the features that were highly discriminative in distinguishing two groups. Therefore, we combined between-group statistical comparison and SVM based individual classification to provide complementary information for assisting clinical TS diagnosis.

5. Conclusion

In the present study, we used probabilistic diffusion tractography and graph theoretical analyses to investigate TS-related changes in the topological organization of WM structural networks. We found that, compared with healthy children, despite TS children showed small-world property, they had a reduced network efficiency in their brain networks, with the most pronounced reduction observed in the visual, default-mode, language and sensorimotor association regions. In addition, two separate network components showing significantly decreased connection strengths were identified by NBS analysis, primarily composed of the parieto-occipital cortex, precuneus and paracentral lobule. Importantly, to enhance our contributions to clinical application, we employed the MK-SVM frameworks to fuse multiple levels of network topological properties as features for accurate classification of individuals, achieving high accuracy of 86.47%. Together, our results suggest a disrupted integrity in the large-scale brain systems in TS and provide structural insights into the brain networks of TS children. The present study may extend our understanding of how structural disruptions of neuronal circuits link to the pathophysiology of TS. The most discriminative network topological features for classification will be potential quantitative neuroimaging biomarkers for assisting the clinical TS diagnosis.

Acknowledgements

We thank Dr. Hao Huang at University of Pennsylvania for consultation and support on MR pulse sequences.

This work was supported by National Natural Science Foundation of China (91520202, 61271151, 31271161), Youth Innovation Promotion Association CAS and Beijing Municipal Administration of

Hospitals Incubating Program (PX2016035)，Beijing health system top level health technical personnel training plan (2015-3-082).

References

Basser, P.J., Mattiello, J., LeBihan, D. (1994a) Estimation of the effective self-diffusion tensor from the NMR spin echo. Journal of magnetic resonance. Series B, 103:247-54.

Basser, P.J., Mattiello, J., LeBihan, D. (1994b) MR diffusion tensor spectroscopy and imaging. Biophys J, 66:259-67.

Basser, P.J., Pajevic, S., ., Pierpaoli, C., ., Duda, J., ., Aldroubi, A., . (2000) In vivo fiber tractography using DT-MRI data. Magnetic resonance in medicine, 44:625-632.

Behrens, T.E., Berg, H.J., Jbabdi, S., Rushworth, M.F., Woolrich, M.W. (2007) Probabilistic diffusion tractography with multiple fibre orientations: What can we gain? Neuroimage, 34:144-55.

Benjamini, Y., Hochberg, Y. (2015) Controlling The False Discovery Rate - A Practical And Powerful Approach To Multiple Testing. Journal of the Royal Statistical Society, 57:289-300.

Bohlhalter, S., Goldfine, A., Matteson, S., Garraux, G., Hanakawa, T., Kansaku, K., Wurzman, R., Hallett, M. (2006) Neural correlates of tic generation in Tourette syndrome: an event-related functional MRI study. Brain, 129:2029-37.

Bullmore, E., Sporns, O. (2009) Complex brain networks: graph theoretical analysis of structural and functional systems. Nat Rev Neurosci, 10:186-98.

Buse, J., Beste, C., Herrmann, E., Roessner, V. (2015) Neural correlates of altered sensorimotor gating in boys with Tourette Syndrome: A combined EMG/fMRI study. The world journal of biological psychiatry : the official journal of the World Federation of Societies of Biological Psychiatry:1-11.

Cao, Q., Shu, N., An, L., Wang, P., Sun, L., Xia, M.R., Wang, J.H., Gong, G.L., Zang, Y.F., Wang, Y.F., He, Y. (2013) Probabilistic diffusion tractography and graph theory analysis reveal abnormal white matter structural connectivity networks in drug-naive boys with attention deficit/hyperactivity disorder. J Neurosci, 33:10676-87.

Cavanna, A.E. (2007) The precuneus and consciousness. CNS spectrums, 12:545-52.

Cavanna, A.E., Seri, S. (2013) Tourette's syndrome. Bmj, 347:67-71.

Chen, Y.F. (2002) Chinese classification of mental disorders (CCMD-3): towards integration in international classification. Psychopathology, 35:171.

Cheng, B., Braass, H., Ganos, C., Treszl, A., Biermann-Ruben, K., Hummel, F.C., Muller-Vahl, K., Schnitzler, A., Gerloff, C., Munchau, A., Thomalla, G. (2014) Altered intrahemispheric structural connectivity in Gilles de la Tourette syndrome. NeuroImage. Clinical, 4:174-81.

Cherine, F., Uicheul, Y., Samir, D., Oliver, L., John, C., Rozie, A., Guy, R., Paul, S., Kirk, F., Catherine, B. (2010) Somatosensory-motor bodily representation cortical thinning in Tourette: effects of tic severity, age and gender. Cortex; a journal devoted to the study of the nervous system and behavior, 46:750-60.

Church, J.A., Fair, D.A., Dosenbach, N.U.F., Cohen, A.L., Miezin, F.M., Petersen, S.E., Schlaggar, B.L. (2009) Control networks in paediatric Tourette syndrome show immature and anomalous

patterns of functional connectivity. Brain, 132:225-238.

Cortes, C., Vapnik, V. (1995) Support-vector networks. Mach Learn, 20:273-297.

Cui, Y., Jin, Z., Chen, X., He, Y., Liang, X., Zheng, Y. (2014) Abnormal baseline brain activity in drug-naive patients with Tourette syndrome: a resting-state fMRI study. Frontiers in human neuroscience, 7:913.

Dai, D., He, H., Vogelstein, J.T., Hou, Z. (2013) Accurate prediction of AD patients using cortical thickness networks. Machine Vision & Applications, 24:1445-1457.

Dai, D., Wang, J., Hua, J., He, H. (2012) Classification of ADHD children through multimodal Magnetic Resonance Imaging. Frontiers in Systems Neuroscience, 6:63-63.

Felling, R.J., Singer, H.S. (2011) Neurobiology of tourette syndrome: current status and need for further investigation. Journal of Neuroscience the Official Journal of the Society for Neuroscience, 31:12387-95.

Ganos, C., Kahl, U., Brandt, V., Schunke, O., Baumer, T., Thomalla, G., Roessner, V., Haggard, P., Munchau, A., Kuhn, S. (2014) The neural correlates of tic inhibition in Gilles de la Tourette syndrome. Neuropsychologia, 65:297-301.

Golden, G.S. (1977) The effect of central nervous system stimulants on Tourette syndrome. Ann Neurol, 2:69–70.

Gong, G., He, Y., Concha, L., Lebel, C., Gross, D.W., Evans, A.C., Beaulieu, C. (2009a) Mapping anatomical connectivity patterns of human cerebral cortex using in vivo diffusion tensor imaging tractography. Cereb Cortex, 19:524-36.

Gong, G., Rosa-Neto, P., Carbonell, F., Chen, Z.J., He, Y., Evans, A.C. (2009b) Age- and gender-related differences in the cortical anatomical network. J Neurosci, 29:15684-93.

Greene, D.J., Church, J.A., Dosenbach, N.U.F., Nielsen, A.N., Adeyemo, B., Nardos, B., Petersen, S.E., Black, K.J., Schlaggar, B.L. (2016) Multivariate pattern classification of pediatric Tourette syndrome using functional connectivity MRI. Developmental Science.

Greicius, M.D., Kaustubh, S., Vinod, M., Dougherty, R.F. (2009) Resting-state functional connectivity reflects structural connectivity in the default mode network. Cereb Cortex, 19:72-78.

Guyon, I., Weston, J., Barnhill, S., Vapnik, V. (2002) Gene selection for cancer classification using support vector machines. Mach Learn, 46:389-422.

Hagmann, P., Kurant, M., Gigandet, X., Thiran, P., Wedeen, V.J., Meuli, R., Thiran, J.P. (2007) Mapping human whole-brain structural networks with diffusion MRI. Plos One, 2:e597.

He, Y., Dagher, A., Chen, Z., Charil, A., Zijdenbos, A., Worsley, K., Evans, A. (2009) Impaired small-world efficiency in structural cortical networks in multiple sclerosis associated with white matter lesion load. Brain, 132:3366-79.

Hong, S.B., Zalesky, A., Fornito, A., Park, S., Yang, Y.H., Park, M.H., Song, I.C., Sohn, C.H., Shin, M.S., Kim, B.N., Cho, S.C., Han, D.H., Cheong, J.H., Kim, J.W. (2014) Connectomic disturbances in attention-deficit/hyperactivity disorder: a whole-brain tractography analysis. Biol Psychiatry, 76:656-63.

Horn, A., Ostwald, D., Reisert, M., Blankenburg, F. (2014) The structural-functional connectome and the default mode network of the human brain. Neuroimage, 102 Pt 1:142-51.

Humphries, M.D., Prescott, T.J. (2006) The brainstem reticular formation is a small-world, not scale-free, network. Proceedings of the Royal Society B Biological Sciences, 273:: 503–511.

Iturria-Medina, Y., Sotero, R.C., Canales-Rodriguez, E.J., Aleman-Gomez, Y., Melie-Garcia, L. (2008) Studying the human brain anatomical network via diffusion-weighted MRI and Graph Theory.

Neuroimage, 40:1064-76.

Jie, B., Zhang, D., Gao, W., Wang, Q., Wee, C.Y., Shen, D. (2014) Integration of network topological and connectivity properties for neuroimaging classification. IEEE transactions on bio-medical engineering, 61:576-89.

Jin, Y., Wee, C.Y., Shi, F., Thung, K.H., Ni, D., Yap, P.T., Shen, D. (2015) Identification of infants at high-risk for autism spectrum disorder using multiparameter multiscale white matter connectivity networks. Human brain mapping.

Leckman, J.F., Riddle, M.A., Hardin, M.T., Ort, S.I., Swartz, K.L., Stevenson, J., Cohen, D.J. (1989) The Yale Global Tic Severity Scale: initial testing of a clinician-rated scale of tic severity. J Am Acad Child Adolesc Psychiatry, 28:566-73.

Li, Y., Jewells, V., Kim, M., Chen, Y., Moon, A., Armao, D., Troiani, L., Markovic-Plese, S., Lin, W., Shen, D. (2013) Diffusion tensor imaging based network analysis detects alterations of neuroconnectivity in patients with clinically early relapsing-remitting multiple sclerosis. Human brain mapping, 34:3376-91.

Liakakis, G., Nickel, J., Seitz, R.J. (2011) Diversity of the inferior frontal gyrus--a meta-analysis of neuroimaging studies. Behavioural brain research, 225:341-7.

Liu, F., Wee, C.Y., Chen, H., Shen, D. (2014) Inter-modality relationship constrained multi-modality multi-task feature selection for Alzheimer's Disease and mild cognitive impairment identification. Neuroimage, 84:466-75.

Liu, Y., Duan, Y.Y., He, Y., Wang, J., Xia, M.R., Yu, C.S., Dong, H.Q., Ye, J., Butzkueven, H., Li, K.C., Shu, N. (2013a) Altered Topological Organization Of White Matter Structural Networks In Patients With Neuromyelitis Optica. Mult Scler J, 19:666-667.

Liu, Y., Miao, W., Wang, J., Gao, P., Yin, G., Zhang, L., Lv, C., Ji, Z., Yu, T., Sabel, B.A., He, H., Peng, Y. (2013b) Structural abnormalities in early Tourette syndrome children: a combined voxel-based morphometry and tract-based spatial statistics study. Plos One, 8:e76105.

Liu, Y., Peng, Y., Gao, P., Nie, B. (2011) Volume Changes of Whole Brain Gray and White Matter in Children Patients with Tourette's Syndrome: Evidence from Voxel-Based Morphometry. Pediatric Research, 70:187-187.

Lo, C.Y., Wang, P.N., Chou, K.H., Wang, J., He, Y., Lin, C.P. (2010) Diffusion tensor tractography reveals abnormal topological organization in structural cortical networks in Alzheimer's disease. J Neurosci, 30:16876-85.

Ludolph, A.G., Juengling, F.D., Libal, G., Ludolph, A.C., Fegert, J.M., Kassubek, J. (2006) Grey-matter abnormalities in boys with Tourette syndrome: magnetic resonance imaging study using optimised voxel-based morphometry. The British journal of psychiatry : the journal of mental science, 188:484-5.

Müller-Vahl, K.R., Grosskreutz, J., Prell, T., Kaufmann, J., Bodammer, N., Peschel, T. (2014) Tics are caused by alterations in prefrontal areas, thalamus and putamen, while changes in the cingulate gyrus reflect secondary compensatory mechanisms. Bmc Neurosci, 15:65-70.

Makki, M.I., Behen, M., Bhatt, A., Wilson, B., Chugani, H.T. (2008) Microstructural abnormalities of striatum and thalamus in children with Tourette syndrome. Movement disorders : official journal of the Movement Disorder Society, 23:2349-56.

Marques, P., Soares, J.M., Magalhaes, R., Santos, N.C., Sousa, N. (2015) The Bounds Of Education In The Human Brain Connectome. Sci Rep, 5:12812.

Maslov, S., Sneppen, K. (2002) Specificity and stability in topology of protein networks. Science,

296:910-3.

Miller, A.M., Ravi, B., Xuejun, H., Juan Pablo, S.P., Sobel, L.J., Jun, L., Dongrong, X., Hongtu, Z., M Mallar, C., Kathleen, D. (2010) Enlargement of thalamic nuclei in Tourette syndrome. Archives of general psychiatry, 67:955.

Mink, J.W. (2003) The Basal Ganglia and involuntary movements: impaired inhibition of competing motor patterns. Archives of neurology, 60:1365-8.

Muller-Vahl, K.R., Kaufmann, J., Grosskreutz, J., Dengler, R., Emrich, H.M., Peschel, T. (2009a) Prefrontal and anterior cingulate cortex abnormalities in Tourette Syndrome: evidence from voxel-based morphometry and magnetization transfer imaging. Bmc Neurosci, 10.

Muller-Vahl, K.R., Kaufmann, J., Grosskreutz, J., Dengler, R., Emrich, H.M., Peschel, T. (2009b) Prefrontal and anterior cingulate cortex abnormalities in Tourette Syndrome: evidence from voxel-based morphometry and magnetization transfer imaging. Bmc Neurosci, 10:47.

Neuner, I., Kupriyanova, Y., Stocker, T., Huang, R., Posnansky, O., Schneider, F., Tittgemeyer, M., Shah, N.J. (2010) White-matter abnormalities in Tourette syndrome extend beyond motor pathways. Neuroimage, 51:1184-93.

Neuner, I., Kupriyanova, Y., Stocker, T., Huang, R.W., Posnansky, O., Schneider, F., Shah, N.J. (2011) Microstructure assessment of grey matter nuclei in adult tourette patients by diffusion tensor imaging. Neuroscience letters, 487:22-26.

Neuner, I., Werner, C.J., Arrubla, J., Stöcker, T., Ehlen, C., Wegener, H.P., Schneider, F., Shah, N.J. (2014) Imaging the where and when of tic generation and resting state networks in adult Tourette patients. Frontiers in human neuroscience, 8:67-77.

Oort, E.S.B.V., Walsum, A.M.V.C.V., Norris, D.G. (2013) An investigation into the functional and structural connectivity of the Default Mode Network. Neuroimage, 90:381–389.

Parker, C.S., Deligianni, F., Cardoso, M.J., Daga, P., Modat, M., Dayan, M., Clark, C.A., Ourselin, S., Clayden, J.D. (2014) Consensus between pipelines in structural brain networks. Plos One, 9:e111262-e111262.

Peng, Z., Shi, F., Shi, C., Yang, Q., Chan, R.C., Shen, D. (2014) Disrupted cortical network as a vulnerability marker for obsessive-compulsive disorder. Brain Structure and Function, 219:1801-1812.

Peterson, B.S., Choi, H.A., Hao, X., Amat, J.A., Zhu, H., Whiteman, R., Liu, J., Xu, D., Bansal, R. (2007) Morphologic features of the amygdala and hippocampus in children and adults with Tourette syndrome. Archives of general psychiatry, 64:1281-91.

Peterson, B.S., Staib, L., Scahill, L., Zhang, H., Anderson, C., Leckman, J.F., Cohen, D.J., Gore, J.C., Albert, J., Webster, R. (2001) Regional brain and ventricular volumes in Tourette syndrome. Archives of general psychiatry, 58:427-40.

Peterson, B.S., Thomas, P., Kane, M.J., Scahill, L., Zhang, H.P., Bronen, R., King, R.A., Leckman, J.F., Staib, L. (2003) Basal ganglia volumes in patients with Gilles de la Tourette syndrome. Archives of general psychiatry, 60:415-424.

Plessen, K.J., Gruner, R., Lundervold, A., Hirsch, J.G., Xu, D., Bansal, R., Hammar, A., Lundervold, A.J., Wentzel-Larsen, T., Lie, S.A., Gass, A., Peterson, B.S., Hugdahl, K. (2006) Reduced white matter connectivity in the corpus callosum of children with Tourette syndrome. Journal of child psychology and psychiatry, and allied disciplines, 47:1013-22.

Plessen, K.J., Wentzel-Larsen, T., Hugdahl, K., Feineigle, P., Klein, J., Staib, L.H., Leckman, J.F., Bansal, R., Peterson, B.S. (2004) Altered interhemispheric connectivity in individuals with Tourette's

disorder. Am J Psychiat, 161:2028-2037.

Qi, S., Meesters, S., Nicolay, K., Bm, T.H.R., Ossenblok, P. (2016) Structural Brain Network: What is the Effect of LiFE Optimization of Whole Brain Tractography? Frontiers in Computational Neuroscience, 10.

Retz-Junginger, P., Retz, W., Blocher, D., Stieglitz, R.D., Georg, T., Supprian, T., Wender, P.H., Rosler, M. (2003) [Reliability and validity of the Wender-Utah-Rating-Scale short form. Retrospective assessment of symptoms for attention deficit/hyperactivity disorder]. Der Nervenarzt, 74:987-93.

Robertson, W.C., Kao, A. (2011) Tourette Syndrome and other Tic disorders. Medscape.

Sacchet, M.D., Prasad, G., Folandross, L.C., Thompson, P.M., Gotlib, I.H. (2015) Support Vector Machine Classification of Major Depressive Disorder Using Diffusion-Weighted Neuroimaging and Graph Theory. Frontiers in psychiatry, 6:21.

Scahill, L., Riddle, M.A., McSwiggin-Hardin, M., Ort, S.I., King, R.A., Goodman, W.K., Cicchetti, D., Leckman, J.F. (1997) Children's Yale-Brown Obsessive Compulsive Scale: reliability and validity. J Am Acad Child Adolesc Psychiatry, 36:844-52.

Schultz, R.T., Carter, A.S., Gladstone, M., Scahill, L., Leckman, J.F., Peterson, B.S., Zhang, H., Cohen, D.J., Pauls, D. (1998) Visual-motor integration functioning in children with Tourette syndrome. Neuropsychology, 12:134-45.

Shu, N., Liu, Y., Li, K., Duan, Y., Wang, J., Yu, C., Dong, H., Ye, J., He, Y. (2011) Diffusion tensor tractography reveals disrupted topological efficiency in white matter structural networks in multiple sclerosis. Cereb Cortex, 21:2565-77.

Sowell, E., Kan, E., J, Thompson, P., Bansal, R., Xu, D., Toga, A., Peterson, B. (2008) Thinning of sensorimotor cortices in children with Tourette syndrome. Nat Neurosci, 11:637-639.

Sporns, O., Honey, C.J. (2006) Small worlds inside big brains. Proc Natl Acad Sci U S A, 103:19219-20.

Sporns, O., Tononi, G., Kotter, R. (2005) The human connectome: A structural description of the human brain. PLoS computational biology, 1:e42.

Stokes, A., Bawden, H.N., Camfield, P.R., Backman, J.E., Dooley, J.M. (1991) Peer Problems in Tourettes Disorder. Pediatrics, 87:936-942.

Supekar, K., Musen, M., Menon, V. (2009) Development of large-scale functional brain networks in children. PLoS biology, 7:e1000157.

Supekar, K., Uddin, L.Q., Prater, K., Amin, H., Greicius, M.D., Menon, V. (2010) Development of functional and structural connectivity within the default mode network in young children. Neuroimage, 52:290–301.

Swick, D., Ashley, V., Turken, U. (2011) Are the neural correlates of stopping and not going identical? Quantitative meta-analysis of two response inhibition tasks. Neuroimage, 56(3):1655-1665.

Telesford, Q.K., Joyce, K.E., Hayasaka, S., Burdette, J.H., Laurienti, P.J. (2011) The ubiquity of small-world networks. Brain connectivity, 1:367-75.

Thomas, E., Michael, S., Joern, K., Christoph, S., Thomas, P., Nils, B., Hans Jochen, H., Mircea Ariel, S. (2004) Differentiation of idiopathic Parkinson's disease, multiple system atrophy, progressive supranuclear palsy, and healthy controls using magnetization transfer imaging. Neuroimage, 21:229-35.

Tzourio-Mazoyer, N., Landeau, B., Papathanassiou, D., Crivello, F., Etard, O., Delcroix, N., Mazoyer, B., Joliot, M. (2002) Automated Anatomical Labeling of Activations in SPM Using a Macroscopic Anatomical Parcellation of the MNI MRI Single-Subject Brain. Neuroimage, 15:273-289.

van den Heuvel, M.P., Mandl, R.C., Stam, C.J., Kahn, R.S., Hulshoff Pol, H.E. (2010) Aberrant frontal and temporal complex network structure in schizophrenia: a graph theoretical analysis. J Neurosci, 30:15915-26.

Verstraete, E., Veldink, J.H., Mandl, R.C., van den Berg, L.H., van den Heuvel, M.P. (2011) Impaired structural motor connectome in amyotrophic lateral sclerosis. Plos One, 6:e24239.

Watts, D.J., Strogatz, S.H. (1998) Collective dynamics of 'small-world' networks. Nature, 393:440-442.

Wen, H., Liu, Y., Rekik, I., Wang, S., Chen, Z., Zhang, J., Zhang, Y., Peng, Y., He, H. (2017a) Multi-modal multiple kernel learning for accurate identification of Tourette syndrome children. Pattern Recognition, 63:601-611.

Wen, H., Liu, Y., Wang, J., Rekik, I., Zhang, J., Zhang, Y., Tian, H., Peng, Y., He, H. (2016a) Combining tract- and atlas-based analysis reveals microstructural abnormalities in early Tourette syndrome children. Human brain mapping, 37:1903-19.

Wen, H., Liu, Y., Wang, J., Zhang, J., Peng, Y., He, H. (A diagnosis model for early Tourette syndrome children based on brain structural network characteristics). In; 2016b. International Society for Optics and Photonics. p 97852R-97852R-9.

Wen, H., Liu, Y., Wang, S., Li, Z., Zhang, J., Peng, Y., He, H. (Multi-threshold white matter structural networks fusion for accurate diagnosis of early Tourette syndrome children). In; 2017b. International Society for Optics and Photonics. p 101341Q-101341Q-13.

Wen, H., Liu, Y., Wang, S., Zhang, J., Peng, Y., He, H. (Diffusion Tractography and Graph Theory Analysis Reveal the Disrupted Rich-Club Organization of White Matter Structural Networks in Early Tourette Syndrome Children). In; 2017c. International Society for Optics and Photonics. p 101371E-101371E-12.

Werner, C.J., Stöcker, T., Kellermann, T., Bath, J., Beldoch, M., Schneider, F., Wegener, H.P., Shah, J.N., Neuner, I. (2011) Altered motor network activation and functional connectivity in adult tourette's syndrome. Human brain mapping, 32:2014-26.

Wilson, S.M., Ogar, J.M., Laluz, V., Growdon, M., Jang, J., Glenn, S., Miller, B.L., Weiner, M.W., Gorno-Tempini, M.L. (2009) Automated MRI-based classification of primary progressive aphasia variants. Neuroimage, 47:1558-67.

Wittfoth, M., Bornmann, S., Peschel, T., Grosskreutz, J., Glahn, A., Buddensiek, N., Becker, H., Dengler, R., Muller-Vahl, K.R. (2012) Lateral frontal cortex volume reduction in Tourette syndrome revealed by VBM. Bmc Neurosci, 13:17.

Wolpert, D.M., Goodbody, S.J., Husain, M. (1998) Maintaining internal representations: the role of the human superior parietal lobe. Nat Neurosci, 1:529-33.

Worbe, Y., Malherbe, C., Hartmann, A., Pelegrini-Issac, M., Messe, A., Vidailhet, M., Lehericy, S., Benali, H. (2012) Functional immaturity of cortico-basal ganglia networks in Gilles de la Tourette syndrome. Brain, 135:1937-46.

Worbe, Y., Marrakchi-Kacem, L., Lecomte, S., Valabregue, R., Poupon, F., Guevara, P., Tucholka, A., Mangin, J.F., Vidailhet, M., Lehericy, S., Hartmann, A., Poupon, C. (2015) Altered structural connectivity of cortico-striato-pallido-thalamic networks in Gilles de la Tourette syndrome. Brain, 138:472-82.

Yendiki, A., Koldewyn, K., Kakunoori, S., Kanwisher, N., Fischl, B. (2014) Spurious group differences due to head motion in a diffusion MRI study. Neuroimage, 88:79-90.

Zalesky, A., Fornito, A., Bullmore, E.T. (2010) Network-based statistic: identifying differences in brain networks. Neuroimage, 53:1197-207.

Zhang, D., Liu, X., Chen, J., Liu, B., Wang, J. (2015) Widespread increase of functional connectivity in Parkinson's disease with tremor: a resting-state FMRI study. Frontiers in aging neuroscience, 7:6.

Zhang, J., Wang, J., Wu, Q., Kuang, W., Huang, X., He, Y., Gong, Q. (2011) Disrupted brain connectivity networks in drug-naive, first-episode major depressive disorder. Biol Psychiatry, 70:334-42.

Zhu, Y., Bai, L., Liang, P., Kang, S., Gao, H., Yang, H. (2016) Disrupted brain connectivity networks in acute ischemic stroke patients. Brain imaging and behavior.

Zhu, Z., Fan, Y., Feng, G., Huang, R., Wang, S. (2013) Large scale brain functional networks support sentence comprehension: evidence from both explicit and implicit language tasks. Plos One, 8:-.

Zhu, Z., Zhang, J.X., Wang, S., Xiao, Z., Huang, J., Chen, H.C. (2009) Involvement of left inferior frontal gyrus in sentence-level semantic integration. Neuroimage, 47:756-63.

Figure Legends

Figure 1. **The flowchart for constructing the WM structural network using diffusion MRI data.**

Figure 2. **The nested cross-validation strategy used in our study.** (A) The flow chart of the nested CV strategy. The feature selection is implemented on the training set, rather than entire dataset. The performance is evaluated on independent test set in outer CV, which may avoid the overfitting problem. (B) The detailed explanation of the inner CV. In the inner CV, the training set is further divided into estimation set and validation set, the SVM parameters was estimated using a grid search method on the estimation set, the validation set is used to assess the optimal SVM parameters.

Figure 3. **Differences in topological properties of WM structural networks between TS patients and controls.** Global metrics of WM structural networks were quantified in controls and TS patients with different probability thresholds. Data points marked with a star indicate a significant group difference ($p < 0.05$) in the global network metric under a corresponding threshold. Both TS patients and controls showed a small-world organization of WM networks characterized by a $\gamma > 1$ and $\lambda \approx 1$. However, compared with controls, TS patients had significantly decreased C_p, λ, global and local efficiency, increased L_p, γ and σ in the WM networks for a series of considered thresholds. HC denotes Healthy controls.

Figure 4. **Distribution of hub regions in the WM structural networks of the control and TS groups and nodes with decreased efficiency in TS children.** (a,b) 3D representations of the hub distributions

in the control (a) and TS (b) groups. The hub nodes are shown in blue and red with node sizes indicating their nodal efficiency values. (c) The disrupted nodes with the significant between-group differences in the regional efficiency are shown in yellow, and the node sizes indicate the t values in t-test. The brain graphs were visualized by using BrainNet Viewer software (http://www.nitrc.org/projects/bnv/). HC denotes Healthy controls. For the abbreviations of nodes, see Table 2.

Figure 5. **Two separate networks that show decreased structural connection strengths in TS children.** Two separate networks showing significantly decreased connectivity were identified in TS group compared with control group (p values < 0.05, NBS corrected). The red nodes and edges represent network 1, primarily comprising the right parieto-occipital, precuneus and cuneus regions. The blue nodes and edges represent network 2, involving the left parieto-occipital, precuneus and bilateral paracentral lobule regions. In the 3D surface view of the components, the edge widths represent the emerging percentage of the WM connections under all 37 thresholds. The nodes and connections were mapped onto the cortical surfaces using BrainNet Viewer software (http://www.nitrc.org/projects/bnv/). For detailed information of the WM connections in the significant NBS components, see Table 6.

Figure 6. **Results of TS classification based on different types of features.** (A) ROC curves of the classification results, which demonstrate the superior performance of using combined features over a single type of features. (B) Brain regions with nodal efficiencies identified as discriminative features

for classification using MKL. The brain graphs were visualized by *volume to surface* function in BrainNet Viewer software. The regional colors with progressive shade (from blue to red) indicate the frequency of being selected by the nested CV procedure. Abbreviation is the same as Table 2.

Table 1. Demographic variables and clinical characteristics of TS patients and normal controls. YGTSS = Yale Global Tic Severity Scale; ADHD = attention deficit hyperactivity disorder; OCD = obsessive compulsive disorder; M = male; F = female. * = two-sample t test. † = χ^2 (chi-square) test.

Characteristics			TS(n=44)	HC(n=41)	p-value
Sex			33M/11F	26M/15F	0.247†
Age			8.98±3.1114	10.27±3.18	0.062*
Concurrent ADHD			7	No	-
Concurrent OCD			No	No	-
YGTSS			51.20±19.38	-	-
Duration (years)			1.73±1.44	-	-
Head Motion	Translation (mm)	x	0.049±0.045	0.051±0.039	0.804*
		y	0.154±0.058	0.163±0.032	0.393*
		z	0.397±0.161	0.362±0.122	0.263*
	Euclidian distance (mm)		0.406±0.111	0.423±0.133	0.546*
	Rotation (10^{-1}×radians)	x	0.023±0.023	0.029±0.025	0.196*
		y	0.010±0.009	0.013±0.009	0.068*
		z	0.010±0.007	0.010±0.006	0.558*
	Mean displacement (mm)	abs	0.810±0.199	0.820±0.133	0.768*
		rel	0.299±0.054	0.300±0.056	0.974*

p>0.05 indicates age, gender and all head motion parameters have no significantly between-group differences and well matched. abs: absolute; rel: relative.

Table 2. Cortical and subcortical regions of interest defined in our study.

Regions	Abbr.	Regions	Abbr.
Precentral gyrus	PreCG	Lingual gyrus	LING
Superior frontal gyrus, dorsolateral	SFGdor	Superior occipital gyrus	SOG
Superior frontal gyrus, orbital part	ORBsup	Middle occipital gyrus	MOG
Middle frontal gyrus	MFG	Inferior occipital gyrus	IOG
Middle frontal gyrus orbital part	ORBmid	Fusiform gyrus	FFG
Inferior frontal gyrus, opercular part	IFGoperc	Postcentral gyrus	PoCG
Inferior frontal gyrus, triangular part	IFGtriang	Superior parietal gyrus	SPG
Inferior frontal gyrus, orbital part	ORBinf	Inferior parietal, but supramarginal and angular gyri	IPL
Rolandic operculum	ROL	Supramarginal gyrus	SMG
Supplementary motor area	SMA	Angular gyrus	ANG
Olfactory cortex	OLF	Precuneus	PCUN
Superior frontal gyrus, medial	SFGmed	Paracentral lobule	PCL
Superior frontal gyrus, medial orbital	ORBsupmed	Caudate nucleus	CAU
Gyrus rectus	REC	Lenticular nucleus, putamen	PUT
Insula	INS	Lenticular nucleus, pallidum	PAL
Anterior cingulate and paracingulate gyri	ACG	Thalamus	THA
Median cingulate and paracingulate gyri	DCG	Heschl gyrus	HES
Posterior cingulate gyrus	PCG	Superior temporal gyrus	STG
Hippocampus	HIP	Temporal pole: superior temporal gyrus	TPOsup
Parahippocampal gyrus	PHG	Middle temporal gyrus	MTG
Amygdala	AMYG	Temporal pole: middle temporal gyrus	TPOmid
Calcarine fissure and surrounding cortex	CAL	Inferior temporal gyrus	ITG
Cuneus	CUN		

Table 3.Group comparisons of AUC values (%) of global network properties.

	S_p	E_{glob}	E_{loc}	L_p	C_p	λ	γ	σ
HC	3.08±0.18	0.18±0.01	0.2±0.02	141.88±8.91	0.62±0.05	11.8±0.28	82.78±6.61	63.13±4.76
TS	2.99±0.3	0.17±0.02	0.2±0.03	135.78±13.31	0.6±0.07	11.68±0.32	85.02±11.89	65.69±10.42
p value	0.11	0.122	0.498	0.016*	0.17	0.061	0.294	0.154

Two sample t-tests were used to determine the differences in the global network properties between groups. Values were the AUC values (mean ± SD) of global network properties in each group.*$p < 0.05$.

Table 4. Hub regions of WM networks in control and TS groups. E_{nodal} represents the AUC value (%) of the nodal efficiency across thresholds.

HC			**TS**		
Hub regions	Category	mean E_{nodal}	Hub regions	Category	mean E_{nodal}
ACG.L	Cingulate	0.215	**ACG.L**	Cingulate	0.211
			ACG.R	Cingulate	0.206
DCG.L	Cingulate	0.222	**DCG.L**	Cingulate	0.216
DCG.R	Cingulate	0.226	**DCG.R**	Cingulate	0.222
PCG.L	Cingulate	0.219	**PCG.L**	Cingulate	0.211
PCG.R	Cingulate	0.222	**PCG.R**	Cingulate	0.215
CUN.L	Occipital	0.232	**CUN.L**	Occipital	0.222
CUN.R	Occipital	0.233	**CUN.R**	Occipital	0.227
SOG.L	Occipital	0.223	**SOG.L**	Occipital	0.214
SOG.R	Occipital	0.218	**SOG.R**	Occipital	0.209
MOG.L	Occipital	0.216	**MOG.L**	Occipital	0.207
PCUN.L	Parietal	0.233	**PCUN.L**	Parietal	0.223
PCUN.R	Parietal	0.232	**PCUN.R**	Parietal	0.225

Table 5. Brain regions with significant between-group differences in nodal efficiency. E_{nodal} represents the AUC values (mean ± SD) (%) of the nodal efficiency of each group.

		E_{nodal}		
Regions	Category	HC	TS	p value
IFGoperc.L	Frontal	0.178±0.016	0.169±0.025	0.035
IFGtriang.L	Frontal	0.181±0.016	0.171±0.025	0.026
HIP.L	Temporal	0.159±0.015	0.151±0.019	0.024
LING.L	Occipital	0.191±0.015	0.183±0.023	0.044
IOG.L	Occipital	0.19±0.015	0.18±0.022	0.022
IOG.R	Occipital	0.166±0.014	0.156±0.02	0.012
FFG.L	Temporal	0.204±0.015	0.194±0.024	0.024
SPG.L	Parietal	0.195±0.017	0.182±0.03	0.019
SPG.R	Parietal	0.165±0.019	0.154±0.03	0.046
IPL.L	Parietal	0.21±0.018	0.198±0.031	0.041
SMG.L	Parietal	0.183±0.017	0.172±0.028	0.028

Table 6. The strengths, percentages, and frequencies of decreased NBS structural connections within two separate white matter networks across all 37 thresholds.

Connection	Connection strengths		Threshold Range	Percentage
	Control	TS		(frequency)
Network 1:				
Cuneus_R ↔ Occipital_Sup_R	0.177±0.016	0.166±0.013	0.02-0.05, 0.0575-0.6, 0.08-0.1	64.86%(24)
Occipital_Sup_R ↔ Occipital_Mid_R	0.174±0.017	0.163±0.019	0.02-0.05, 0.0575-0.6, 0.08-0.1	64.86%(24)
Occipital_Sup_R ↔ Parietal_Sup_R	0.064±0.013	0.058±0.017	0.02-0.05	35.14%(13)
Lingual_R ↔ Occipital_Inf_R	0.050±0.010	0.040±0.010	0.01-0.0125, 0.0575-0.6	10.81%(4)
Occipital_Mid_R ↔ Occipital_Inf_R	0.076±0.011	0.066±0.014	0.0575-0.6	5.41%(2)
Parietal_Sup_R ↔ Precuneus_R	0.063±0.009	0.058±0.014	0.05	2.70%(1)
Network 2:				
Parietal_Sup_L ↔ Precuneus_L	0.076±0.011	0.069±0.014	0.015-0.0175	5.41%(2)
Precuneus_L ↔ Paracentral_Lobule_L	0.042±0.010	0.035±0.008	0.015-0.0175	5.41%(2)
Paracentral_Lobule_L ↔ Paracentral_Lobule_R	0.031±0.010	0.026±0.008	0.015-0.0175	5.41%(2)
Occipital_Mid_L ↔ Parietal_Sup_L	0.030±0.010	0.026±0.006	0.0175	2.70%(1)

Connection strengths: mean (±SD) values of the connection strength (probability) in each group. Threshold Range/Percentage (frequency): the values represent the threshold range, the emerging percentage and times of the WM connections under all 37 thresholds (0.01–0.1, interval = 0.0025) in which the NBS components were statistically significant. For the abbreviations of the regions, see Table 2.

Table 7. Classification performances of all methods in percentage.

Feature	Accuracy(%)	Sensitivity(%)	Specificity(%)	ROC AUC(%)
Global properties	63.24±3.54	64.32±5.22	62.07±5.57	64.09±2.87
Nodal efficiencies	60.76±3.82	65.11±4.96	56.10±7.51	62.18±3.18
Pair-wise SC	78.18±2.82	67.95±6.91	89.15±3.01	88.77±1.57
Combining features	86.47±3.71	85.57±4.38	87.44±4.13	92.62±3.35

Table 8. The top ten features for each kind of network properties selected by the nested CV procedure as the most discriminative for TS classification.

Global feature			Nodal feature			Edge feature		
Property	Counts	Freq	Region	Counts	Freq	Connection	Counts	Freq
λ (T=0.09)*	198	99.0%	IOG.R*	194	97.0%	ORBinf.R-PreCG.R	200	100.0%
C_p (T=0.045)*	190	95.0%	PUT.R	188	94.0%	IFGtriang.R-MFG.R	200	100.0%
σ (T=0.0575)*	190	95.0%	HIP.L*	175	87.5%	PCG.L-INS.L	197	98.5%
E_{glob} (T=0.085)*	156	78.0%	IFGtriang.L*	150	75.0%	CUN.R-SOG.R*	192	96.0%
σ (T=0.075)*	155	77.5%	SPG.L*	123	61.5%	CUN.R-DCG.R	190	95.0%
C_p (T=0.0425)*	154	77.0%	IOG.L*	118	59.0%	DCG.R-PCG.R	189	94.5%
λ (T=0.095)*	136	68.0%	FFG.L*	108	54.0%	CAL.L-OLF.R	188	94.0%
E_{loc} (T=0.045)*	130	65.0%	AMYG.R	107	53.5%	MOG.L-SPG.L*	185	92.5%
γ (T=0.095)*	130	65.0%	IFGoperc.L*	102	51.0%	SOG.R-ORBsupmed.L	185	92.5%
E_{loc} (T=0.04)*	128	64.0%	SPG.R*	85	42.5%	SOG.R-MOG.R*	184	92.0%

Counts: the counts of each feature selected by our proposed method over the 20 rounds nested 10-fold CV. Freq: the frequency of being selected, equals Counts/total times in 20 rounds nested 10-fold CV (200 times). *: Feature marked with a star (*) indicates it was significantly altered in between-groups statistical comparison.

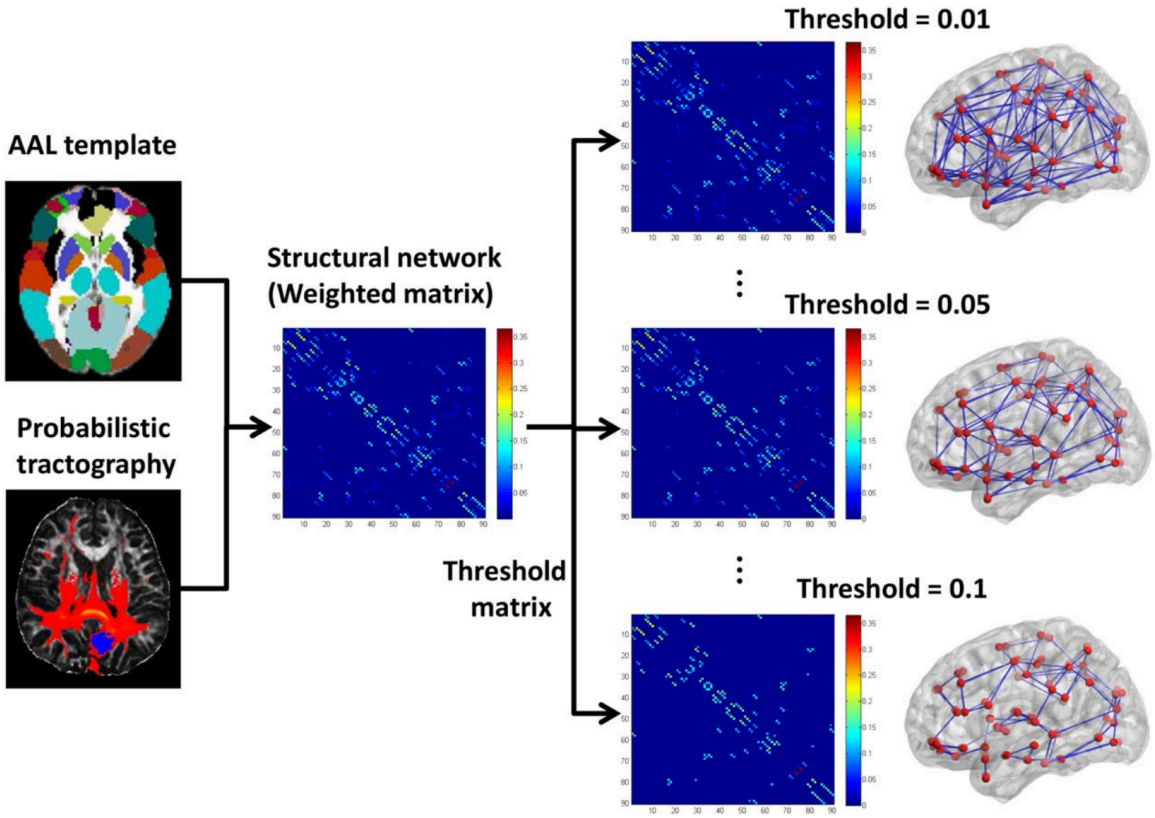

Figure 1. The flowchart for the construction of the functional structural network by rs-fMRI data.

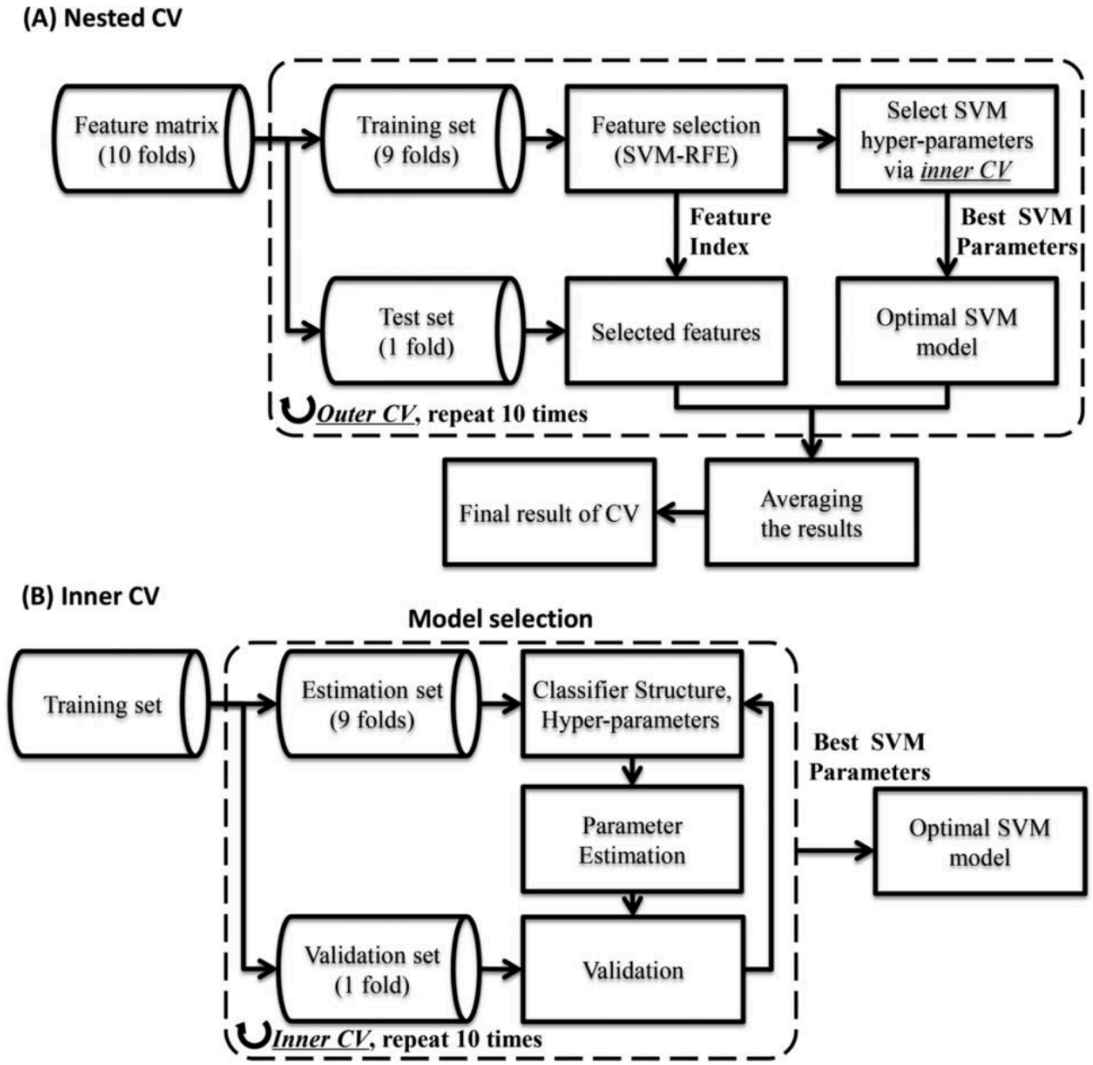

Figure 2. The flow chart of the nested CV procedure in our classification framework.

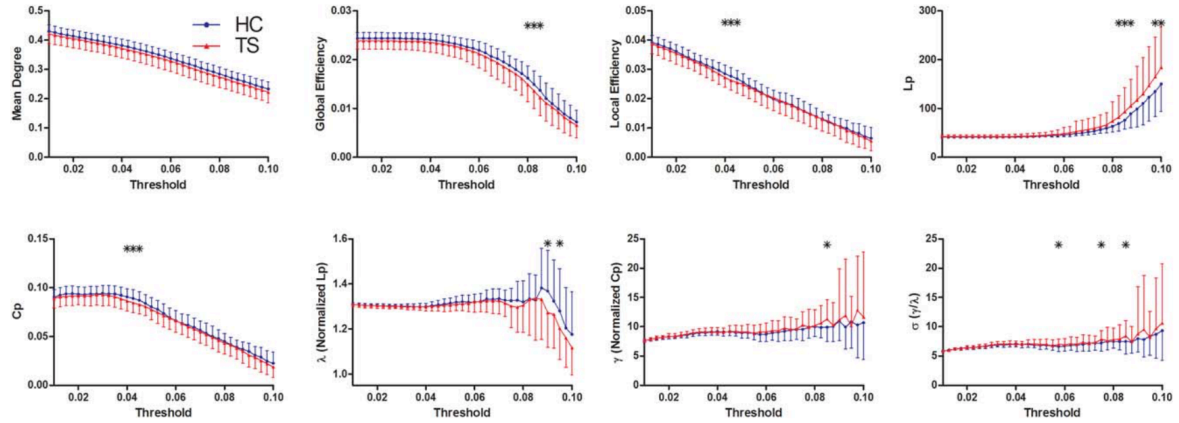

Figure 3. Differences in topological properties of WM structural networks between TS patients and controls. Global metrics of WM structural networks were quantified in controls and TS patients with different probability thresholds. Data points marked with a star indicate a significant group difference ($P < 0.05$) in the global network metric under a corresponding threshold. Both TS patients and controls showed a small-world organization of WM networks characterized by a $\gamma > 1$ and $\lambda \approx 1$. However, compared with controls, TS patients had significantly decreased C_p, λ, global and local efficiency, increased L_p, γ, and σ in the WM networks for a series of considered thresholds. HC, healthy controls.

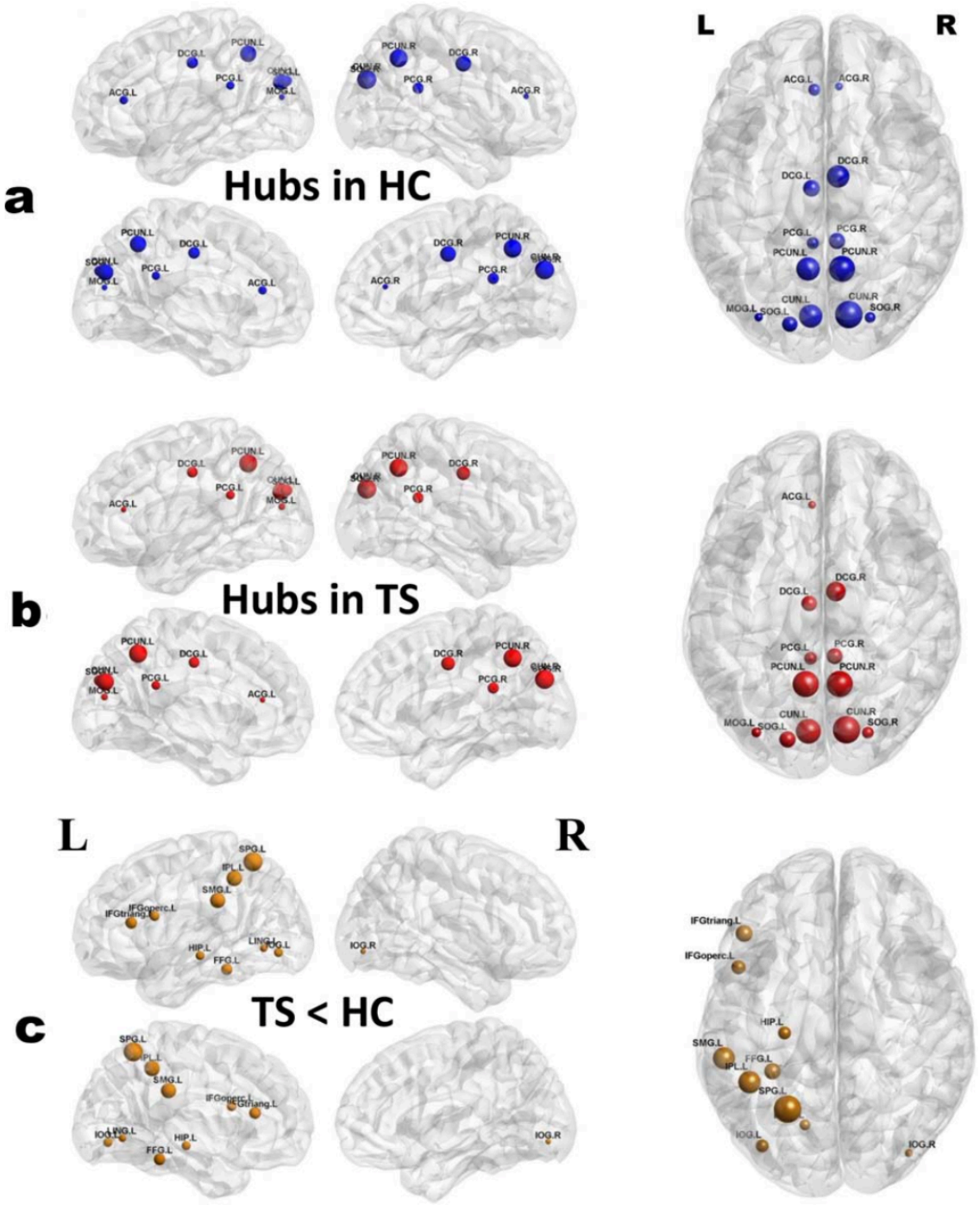

Figure 4. Distribution of hub regions in the WM structural networks of the control and TS groups and nodes with decreased efficiency in TS children. (a,b) 3D representations of the hub distributions in the control (a) and TS (b) groups. The hub nodes are shown in blue and red with node sizes indicating their nodal efficiency values. (c) The disrupted nodes with the significant between-group differences in the regional efficiency are shown in yellow, and the node sizes indicate the t values in t test. The brain graphs were visualized by using BrainNet Viewer software (http://www.nitrc.org/projects/bnv/). HC, healthy controls. For the abbreviations of nodes, see Table II.

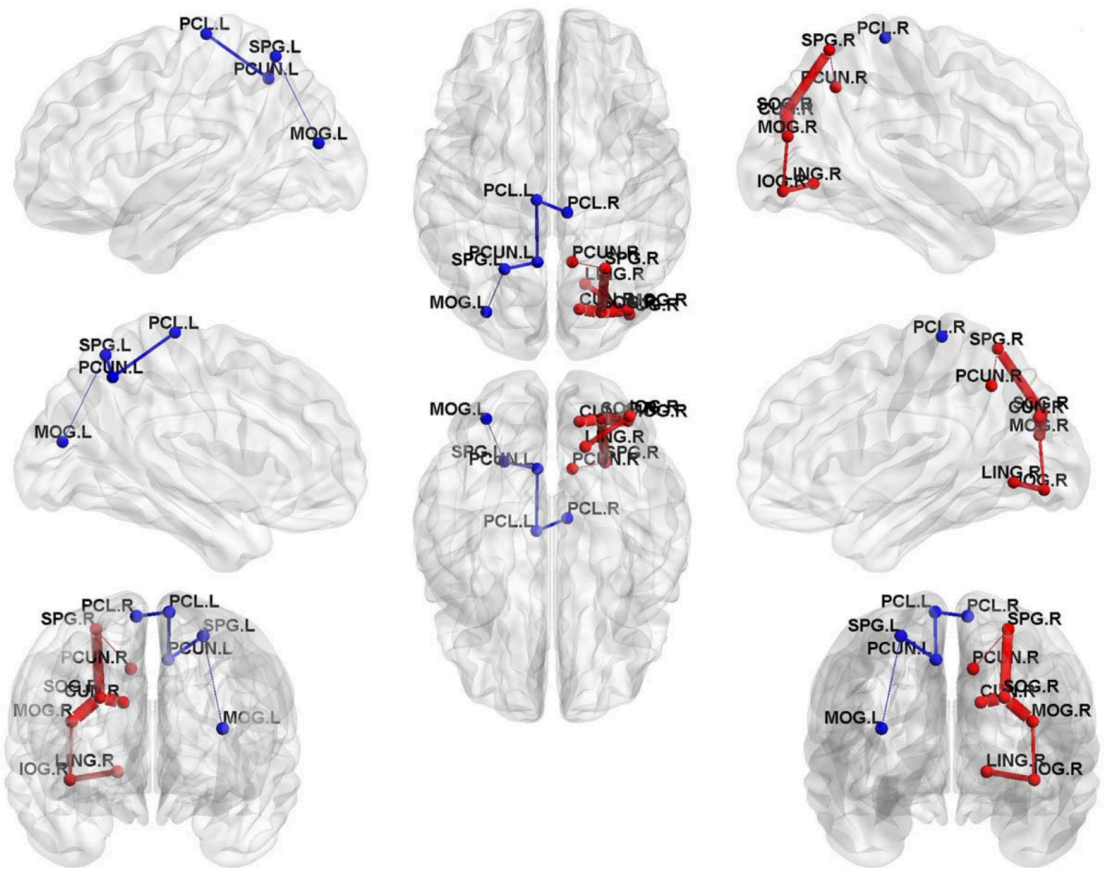

Figure 5. Two separate networks that show decreased structural connection strengths in TS children. Two separate networks showing significantly decreased connectivity were identified in TS group com- pared with control group (P values < 0.05, NBS corrected). The red nodes and edges represent network 1, primarily comprising the right parieto-occipital, precuneus, and cuneus regions. The blue nodes and edges represent network 2, involving the left parieto-occipital, precuneus, and bilateral paracentral lobule regions. In the 3D surface view of the components, the edge widths represent the emerging percentage of the WM connections under all 37 thresholds. The nodes and connections were mapped onto the cortical surfaces using BrainNet Viewer software (http:// www.nitrc.org/projects/bnv/). For detailed information of the WM connections in the significant NBS components, see Table VI.

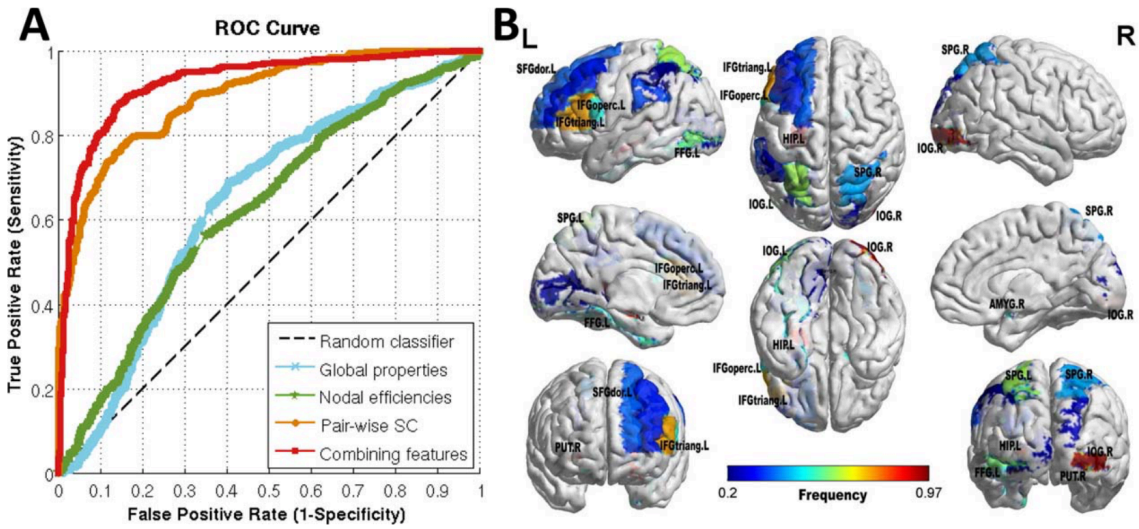

Figure 6. Results of TS classification based on different types of features. (A) ROC curves of the classification results, which demonstrate the superior performance of using combined features over a single type of features. (B) Brain regions with nodal efficiencies identified as discriminative features for classification using MKL. The brain graphs were visualized by volume to surface function in Brain- Net Viewer software. The regional colors with progressive shade (from blue to red) indicate the frequency of being selected by the nested CV procedure. Abbreviation is the same as Table II.